PARAMETER OPTIMIZATION FOR REACTION TORQUE OBSERVER BASED MOTION SYSTEMS

W. M. T. G. Wijewardhana

198041X

Master of Science (Major Component Research)

Department of Electrical Engineering
Faculty of Engineering

University of Moratuwa
Sri Lanka

July 2024

PARAMETER OPTIMIZATION FOR REACTION TORQUE OBSERVER BASED MOTION SYSTEMS

W. M. T. G. Wijewardhana

198041X

Thesis submitted in partial fulfillment of the requirements for the degree
Master of Science (Major Component Research)

Department of Electrical Engineering
Faculty of Engineering

University of Moratuwa
Sri Lanka

July 2024

DECLARATION

I declare that this is my own work and this Thesis does not incorporate without acknowledgement any material previously submitted for a Degree or Diploma in any other University or Institute of higher learning and to the best of my knowledge and belief it does not contain any material previously published or written by another person except where the acknowledgement is made in the text. I retain the right to use this content in whole or part in future works (such as articles or books).

Signature: ***UOM Verified Signature*** Date: 29/ 07/2024

The supervisor should certify the Thesis with the following declaration.

The above candidate has carried out research for the Master of Science (Major Component Research) Thesis under my supervision. I confirm that the declaration made above by the student is true and correct.

Name of Supervisor: Dr. A. M. Harsha S. Abeykoon

Signature of the Supervisor: Date:

30/7/2024

DEDICATION

This study is wholeheartedly dedicated to my beloved parents and my wife. Their endless love, unwavering support, and constant encouragement have been my pillars of strength throughout this journey. Without their guidance and belief in me, this achievement would not have been possible. Thank you for always being there for me.

ACKNOWLEDGEMENT

This Master of Science thesis is a requirement for partial completion of the degree program at the University of Moratuwa. It is a compilation of research work conducted at the Control and Robotics Laboratory, within the Electrical Engineering Department of the Faculty of Engineering at the University of Moratuwa, Sri Lanka.

I am deeply grateful to my supervisor, Dr. A. M. Harsha S. Abeykkon, for his unwavering guidance and support throughout the research process. His expertise in the field of Electrical Engineering was invaluable in shaping my research and ensuring that it met the highest standards.

Furthermore, I would like to acknowledge the significant contribution of my post-graduate colleague, Mr. K. D. M. Jayawardhana, who provided me with vital assistance during challenging tasks. His technical expertise and encouragement were vital in keeping me motivated and focused throughout the research.

The Electrical Engineering Department at the University of Moratuwa was a constant source of support during the research activity. I would like to express my gratitude to all members of the department who provided me with the resources and assistance needed to carry out my research.

I also want to express my sincere appreciation to everyone who has assisted me in my life, particularly my parents, Mr. W. M. G. S. Wijewardana and Mrs. E. D. S. M. Wijewardana, for their unwavering support and encouragement. My wife, Mrs. K. A. C. S. Kodisinghe, also deserves special thanks for her understanding and support throughout the research.

Finally, I would like to extend my gratitude to all individuals who contributed to the successful completion of this thesis, whether through their technical expertise, encouragement, or support. I apologize for any inadvertent omissions in mentioning them personally and am grateful for their contributions to this research.

ABSTRACT

This thesis investigates the use of reaction torque observer (RTOB)-based controllers as a solution for the challenges associated with force sensors in motion systems. RTOB-based controllers provide significant advantages, including variable bandwidth, the capability to estimate unknown disturbances, and the feedback of disturbances to enhance system robustness. The model-based architecture of this approach necessitates precise parameter estimation, which is a critical aspect of stability analysis. Consequently, this thesis proposes a rapid and accurate method for parameter estimation, aiming to minimize computational expense.

A comprehensive stability analysis is conducted to determine the conditions under which RTOB-based controllers maintain robust performance. The stability study considers various environmental conditions and controller settings to provide guidelines for achieving optimal stability. Additionally, the study explores the effects of external vibrations on system performance and the effectiveness of the controller in suppressing these vibrations.

The findings demonstrate that RTOB-based controllers can significantly improve system performance by providing variable bandwidth, enhancing robustness, and accurately estimating unknown disturbances. The proposed optimization of controller parameters and the novel parameter estimation technique offer valuable insights for scientists and engineers to implement this strategy in various motion systems.

Overall, this research advances the field of motion systems by providing a viable alternative to traditional force sensors and emphasizing the importance of vibration suppression and stability analysis. The outcomes have implications for the design and development of motion systems across different applications, enhancing their overall effectiveness and reliability.

Keywords: Disturbance Observer, Reaction Torque Observer, Parameter estimation, Stability analysis, Vibration suppression

TABLE OF CONTENTS

LIST OF FIGURES

LIST OF TABLES

LIST OF APPENDICES

CHAPTER 1

INTRODUCTION

Motion systems are pivotal in a myriad of applications across robotics and automation, demanding high precision and reliability for optimal performance and safety. Traditional systems often rely on force sensors to control and monitor motion, which introduces challenges such as increased cost, complexity, and potential for mechanical failures. As a solution, Reaction Torque Observers (RTOBs) have emerged as a cutting-edge alternative, enabling the precise estimation of torque without direct force measurement [1][2]. This technology not only reduces system dependency on cumbersome sensors but also enhances the robustness and adaptability of motion control systems [3].

The global aging population and the subsequent increase in mobility impairments have spurred significant research into advanced motion systems. With an estimated 500 million people worldwide over the age of 65 [4][5], the demand for sophisticated technologies to aid in mobility and rehabilitation is more pressing than ever. Particularly in countries like China, where the proportion of the elderly population is expected to reach 18.2 percentage by 2030, the need for innovative solutions to mobility challenges is critical [6][7].

The development of advanced motion systems using RTOBs is crucial for addressing these needs. However, the effectiveness of these systems hinges on precise parameter optimization, which ensures accurate torque estimation and system responsiveness. This research focuses on enhancing the optimization techniques for RTOBs, aiming to improve the calibration of system parameters such as inertia and friction coefficients, which are vital for maintaining stability and ensuring safety during operation [8].

Robotic systems that interact with humans, such as those used in rehabilitation or assistive technologies, must be particularly compliant and sensitive to human movement. Impedance control strategies, which adjust the robot's response based on the force exerted by and on the human, are central to this interaction. However, achieving a balance between low impedance for safety and high impedance for task accuracy requires sophisticated control algorithms and real-time system adjustments based on accurate motion parameter estimation [9][10].

Current methods for parameter estimation often rely on visual or sensor-based techniques, which can be hampered by environmental variables such as lighting conditions or sensor inaccuracies. Therefore, this thesis proposes the use of advanced numerical methods and RTOB-based approaches to refine the estimation processes, enhancing the efficiency and reducing the computational demand of these systems [11]. This approach is expected to yield significant improvements in the safety, performance, and reliability of motion systems, particularly in applications involving direct human inter-

action. Additionally, a thorough stability analysis is necessary to understand the conditions under which RTOB-based controllers can maintain robust performance. This analysis is particularly important in environments with varying external disturbances and dynamic changes. Addressing these challenges is crucial for optimizing RTOB parameters and ensuring the stability and effectiveness of motion systems.

Furthermore, this research includes a comprehensive study on the suppression of vibrations in motion systems using RTOBs. Effective vibration suppression is vital for maintaining the precision and stability of motion systems, particularly in environments subject to external disturbances. The findings demonstrate that RTOB-based controllers can significantly enhance system performance by providing variable bandwidth, robustness enhancement, and accurate estimation of unknown disturbances.

1.1 Active Compliance Force Controllers and Disturbances

Motion systems are frequently exposed to unknown environmental disturbances as well as disturbances. Gravity, inertia, and friction are frequently responsible for the most significant unknown disturbances. Therefore, the need for reliable contact transition and force tracking control in an unknown or shifting environment has emerged.

The control systems for compliant control are typically designed using force control topology. It is considered that these motion systems have the following challenges [12];

1. Environment in contact altering the overall control system's structure.
2. Attainment of force control robustness.
3. Monitoring reaction force.

For instance, a rehabilitation robot with gravity compensation was created in [13], and the arm of the patient's gravity effect was modeled as a disturbance. The robustness of the system as a whole is increased by compensating for the disturbance brought on by gravity. But neither the patient's arm's weight nor its inertia were estimated. Assuming it is a constant, the inertia of a human arm has already been determined. In rehabilitation systems, this is untrue though because it could alter over time. Additionally, the research in [14] demonstrates that the nature of the environment in contact varies nonlinearly with motion parameters, making the controller design more challenging.

The fundamental method of interacting with humans is stiffness control, which is equivalent to proportional-derivative control [15]. The robot's stiffness is determined by the proportional gain, which must be properly calibrated in relation to the stiffness of the human response. The goal of stiffness control is to produce a static interaction.

Hybrid position/force control [16] or impedance control can be used to provide active compliance [12]. The task space in hybrid position/force control is split into two orthogonal, non-interfering position and force controlled subspaces. According to [10], the objective of an impedance controller is to establish a desired dynamic relationship between the endpoint position and the environmental force. These studies have led to the development of force control using neural networks [17] and contact transition control using acceleration feedback [17]. Thus, the development of novel force control architectures has received significant research attention.

1.2 Force Sensors

The influence of the external environment on the robot is typically measured by a force sensor in force feedback robots. It is crucial that this measurement be accurate. However, it is common knowledge that force sensor readings contain a lot of noise. This is explained in Figure 1.1.

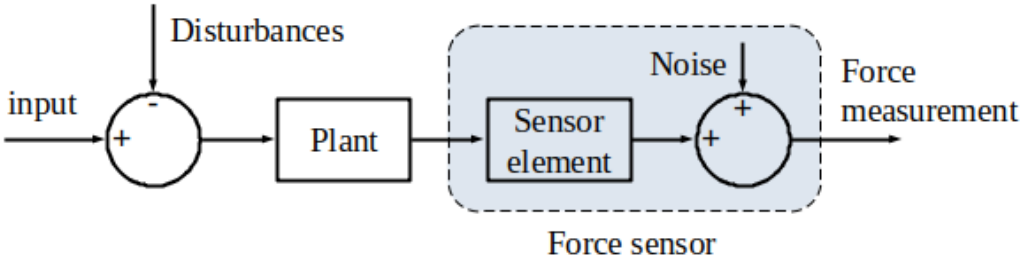

Fig. 1.1: A force sensor attached to a plant

Strain gauges are the most popular sensor type used in force control applications. For an example, consider a rehabilitation robot where the strain gauges need to be fixed so that the entire external torque can be recorded in order to measure the torque applied by a patient. For instance, the muscle-measuring apparatus Kin-Com was used in the research project described in [18]. The weight of the lower leg is determined by a load cell on the link of KinCom. These kinds of arrangements typically have few limitations. The position of the sensor to which the measurement is attached, the sensor's bandwidth, and hysteresis errors in the sensor's deformation are a few typical causes that can strongly affect the measurement. Furthermore, research [6] has shown that it is difficult to achieve force control when using a force sensor as the feedback.

1.3 Observers

Control engineering uses observers or estimators frequently because they can determine the immeasurable parameters. These are utilized in motion control systems to

monitor ambiguous or uncertain parameters, such as disturbances. On the other hand, state estimators calculate the states of the control modal using a mathematical model of the plant [19].

Figure 1.2 illustrates how an observer would be implemented with a real plant.

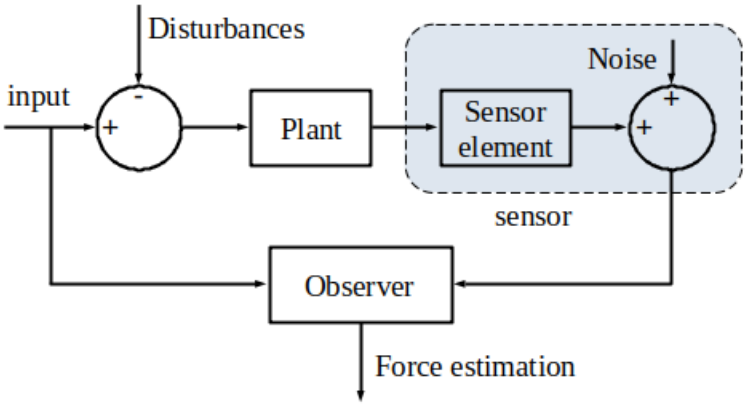

Fig. 1.2: An observer integrated to a plant

1.4 Force Sensorless Force Controllers

The use of force sensors in motion control results in a reduction in control performance. Fortunately, sensorless force control has been made possible [20]. An observer for reaction force estimation is used rather than a force sensor.

The reaction torque observer proposed in [21] is used in numerous applications as a better alternative. It can observe the external torque without force sensors [12]. A force control system does not contain a soft mechanism to separate the robot from its surroundings when the disturbance observer is implemented in a robot. As a result, the robot is given the ability to directly detect external forces. Additionally, employing the disturbance observer results in a force-sensing bandwidth that is quite broad.

The use of the reaction torque observer with the disturbance observer has helped to address the most significant issues with a traditional compliance control system. The research work in [22] provides a concise review of prior work on the impact of disturbance observer and reaction torque observer on the advancement of rehabilitation robots. As a result, the focus of this study can now be more specifically defined as motion systems that employ reaction torque observers as force sensors.

1.5 System Parameters

Force control has been challenging to implement in motion systems when they come into contact with human subjects. One factor that significantly affects this is the unpre-

dictability of the system parameters. For example, system inertia, being a parameter that has a huge impact on system stability, can be subject to variations when the external load or the motion system is in movement. Another crucial element that must be taken into account when designing a force controller is the variations in external impedance that the controller experiences.

It is well known that selecting the ideal stability-to-robustness ratio when designing control systems can be difficult. This becomes worse when it comes to force control systems in rehabilitation robots. The controller must be able to manage changes in external impedance and inertia while maintaining robustness and safety requirements. Numerous studies have shown that the best approach is to equip the controller with the intelligence necessary to estimate the instantaneous parameter changes and to continuously modify the controller's parameters. For instance, a numerical estimation process is used in the research work in [23] to estimate the inertia of an upper limb rehabilitation robot in real time. Recursive Least Squares has proven to be more effective compared to adaptive linear neurons. However, the change in environmental impedance has been neglected. Furthermore, in the aforementioned works, the robotic systems do not adjust to the motion intended by the human, but instead manipulate human limbs directly. In order to ensure safety when directly manipulating human body parts, more information is required and cannot be provided by using a stand-alone compliant controller. In light of this, the main objective of this research project can be further distilled to the parameter optimization for reaction torque observer based motion systems.

1.6 Objectives

The majority of advanced motion control systems, particularly those used in industrial and robotic applications, historically relied on force sensors to monitor interactions and ensure precision. However, the inherent limitations of force sensors, such as their susceptibility to environmental interference and mechanical wear, make compliant control challenging. The adoption of Reaction Torque Observer-based (RTOB) controllers presents a more effective solution to these challenges. RTOBs offer notable advantages over conventional force sensors, including the ability to estimate unknown disturbances, adjustable bandwidth, and the capability to feedback disturbances to enhance system robustness.

Given that these advantages hinge on a model-based architecture, accurate parameter estimation becomes crucial. This research is primarily focused on examining stability variations in RTOB-based motion systems and developing guidelines for fine-tuning controller parameters. The precision of system parameters plays a vital role in stability analysis, making the process of parameter estimation significantly impactful.

Accordingly, this thesis aims to implement a precise and efficient method for pa-

rameter estimation while minimizing computational costs. Additionally, the performance of these motion systems is often affected by high-frequency external vibrations, such as those from infrastructure or mechanical sources, which the controller may mistakenly perceive as reaction forces. Therefore, another key objective of this study is to investigate the RTOB-based controller's ability to suppress such vibrations, further refining its functionality and applicability in various settings.

This research will contribute to the field by enhancing the performance and reliability of RTOB-based motion systems, offering advanced methodologies for parameter optimization, and providing new insights into the dynamic behavior of these systems under various operational conditions.

1.7 Originality

The research on motion control systems has been intensively explored for several years, with many researchers focusing on developing new control strategies, sensor technologies, and mechanical designs to enhance the performance and efficiency of these systems. However, the use of Reaction Torque Observer-based (RTOB) controllers in broader motion systems represents a relatively novel approach that has begun to gain traction in recent years.

A unique aspect of RTOB-based controllers is their capability to estimate unknown disturbances in real-time, which is critical in the context of motion control. Considering that mechanical and robotic systems encounter unpredictable and variable disturbances during operation, the ability to accurately estimate and compensate for these disturbances is essential for optimal functionality.

The aim of this thesis is to explore stability variations in RTOB-based motion systems and develop guidelines for fine-tuning controller parameters. This research will contribute to the current understanding of the stability of these systems and provide insights into how to optimize their performance.

The originality of this thesis lies in several aspects:

1.7.1 Advanced Parameter Estimation

This research focuses on developing a precise yet rapid method for parameter estimation while keeping the computational cost to a minimum. Many existing methods for parameter estimation are computationally intensive and time-consuming. Developing a more efficient and accurate method for parameter estimation will significantly contribute to the field.

1.7.2 Vibration Suppression

The thesis will also investigate the impact of high-frequency external vibrations, such as those from infrastructure or operational environments, on the performance of the RTOB-based controller. This aspect is crucial because vibrations commonly affect real-world applications, and understanding how the controller responds to these disturbances will be critical for developing more robust and reliable motion systems.

1.7.3 Study of Stability

This research significantly contributes to the field by providing a deeper understanding of stability in RTOB-based motion systems. The focus on stability analysis under different operational conditions and disturbances will offer new insights that can guide the design and control of these systems more effectively.

Overall, the originality of this thesis lies in its focus on enhancing the stability of RTOB-based motion control systems, developing a more efficient and accurate method for parameter estimation, and investigating the impact of high-frequency exterior vibrations on controller performance. These contributions will be valuable for improving the performance and reliability of advanced motion systems and advancing the field of motion control technology.

1.8 Thesis Organization

Figure 1.3 depicts the thesis's organizational structure. According to the chapter order, a summary of each chapter is given below.

1.8.1 Chapter 1

This chapter introduces the context of the thesis, focusing on motion control systems. It discusses the limitations of traditional torque sensors and the challenges with robustness in compliance control robots. The concepts of Disturbance Observer (DoB) and Reaction Torque Observer (RTOB) are introduced as solutions to enhance system performance.

The chapter also covers the challenges in modeling these systems and emphasizes how crucial accurate parameter estimation is to their effectiveness. By addressing these topics, the chapter sets the foundation for exploring advanced parameter optimization techniques and their potential benefits across various motion systems.

Overall, Chapter One provides an overview of the essential concepts and challenges, setting the stage for a deeper exploration of optimizing Reaction Torque Observers in subsequent chapters.

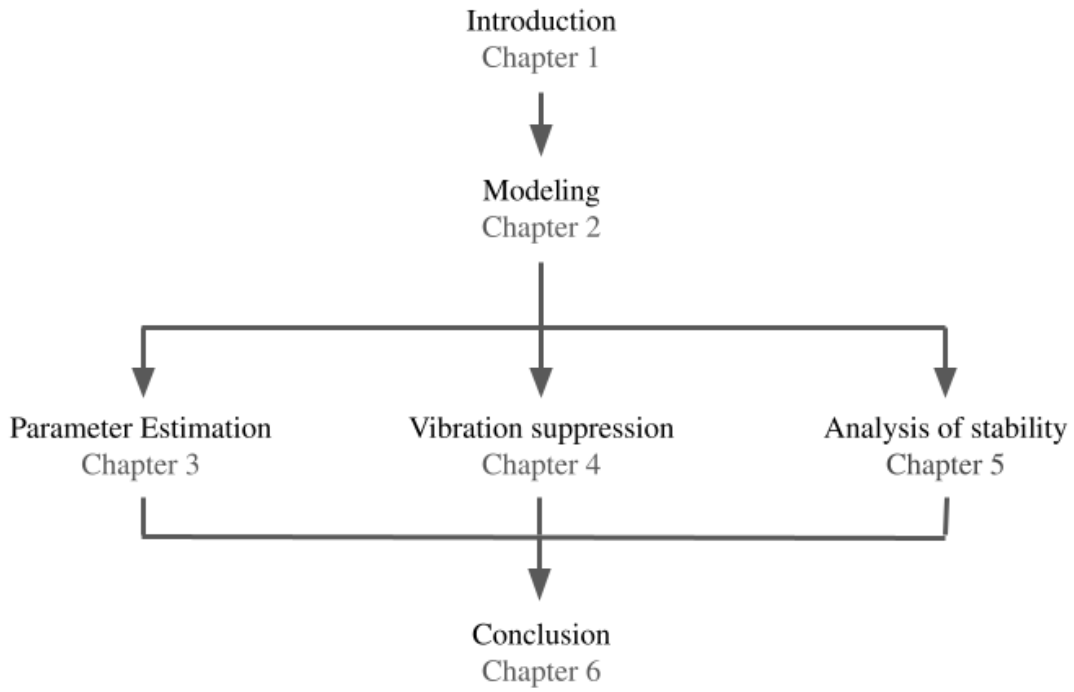

Fig. 1.3: An overview of the thesis

1.8.2 Chapter 2

This chapter presents the modeling of the fundamental control block diagrams that were used in the studies in chapters 3, 4, and 5. It includes models for the reaction torque observer, disturbance observer, and DC motor based on the current controlled architecture.

1.8.3 Chapter 3

A new technique for parameter estimation of small-scale DC motors using a disturbance observer and optimization algorithm is proposed in this chapter. The approach offers a simplified cost function for the disturbance observer based model and accurately estimates the moment of inertia, coefficient of viscous friction, and static friction, which are compared with actual parameters.

1.8.4 Chapter 4

This chapter presents a force control method that utilizes disturbance observers to suppress vibrations in force controllers. The proposed method uses an inner loop disturbance observer and an outer loop reaction torque observer to estimate and compensate for disturbances. Simulation and real-world experiments show that the proposed method outperforms traditional force control methods by effectively suppressing vibrations. Increasing the cutoff frequency of the disturbance observer can further improve

performance, but is limited by sampling time. Disturbance observers are thus shown to be an effective means of suppressing vibrations in force controllers.

1.8.5 Chapter 5

This chapter explores the instability of force controllers that utilize a reaction torque observer (RTOB) and disturbance observer (DoB) to accurately determine environmental impedance. It is commonly assumed that the cutoff frequencies of both observers should always be equal, but this can lead to instability under certain conditions. This chapter proposes a new stability assessment approach and derives a novel stability constraint and guideline. Simulation results confirm the validity of these proposals. The study highlights the importance of considering system dynamics and design constraints when implementing RTOB-based force controllers.

1.8.6 Chapter 6

This chapter provides a comprehensive overview of the key findings and conclusions of the presented thesis. It summarizes the main arguments and contributions, as well as their significance and implications for the field of study. The summary serves as a final reflection on the research undertaken and offers recommendations for future research.

CHAPTER 2

MODELING

2.1 Disturbance Observer and Reaction Torque Observer

Ohinishi et al proposed the Disturbance Observer, which is a robust motion control tool utilized to estimate disturbances that are uncertain or unknown [19] [20].

The main concept behind this disturbance observer is to add an imaginary autonomous dynamical system to the plant that causes the disturbances. Then, an observer is designed to calculate the states of the plant and the disturbance generator. Disturbance rejection is achieved using the estimated disturbance state as feedback [20]. Therefore, the robust enhancement is achieved. To attain the performance objectives, the controller is created to solely take into account the nominal plant. The format of such a control system, having both an inner loop and an outer loop is known as a two-degree of freedom control structure.

A low-pass filter is usually used to handle the casualties in the inner loop. However, the cutoff frequency acts as a significant parameter as it can control the robustness and stability. If the cutoff frequency is set to a higher value, the accuracy of the estimated disturbance is very high. Therefore, the robustness can be enhanced by tuning the cutoff frequency to a higher value. However, the cutoff frequency is limited by the sampling time the controller is implemented.

The selection of the filter as a low-pass filter and an explanation of how cutoff frequency and nominal plant modal dynamics affect robustness are covered in the following section.

2.2 Effects of nominal plant model dynamics and filter derivation

A robust DoB-based control system is depicted in a generalized block diagram in Figure 2.1. Table 2.1 provides a description of the terminology.

The disturbance estimation can be obtained from the difference between the estimated nominal plant input $\hat{u}$ and plant input u, presuming that the system depicted in Figure 2.1 is a single input single output system (SISO). The relevant transfer functions can be derived as in Equations 2.1, 2.2, and 2.3.

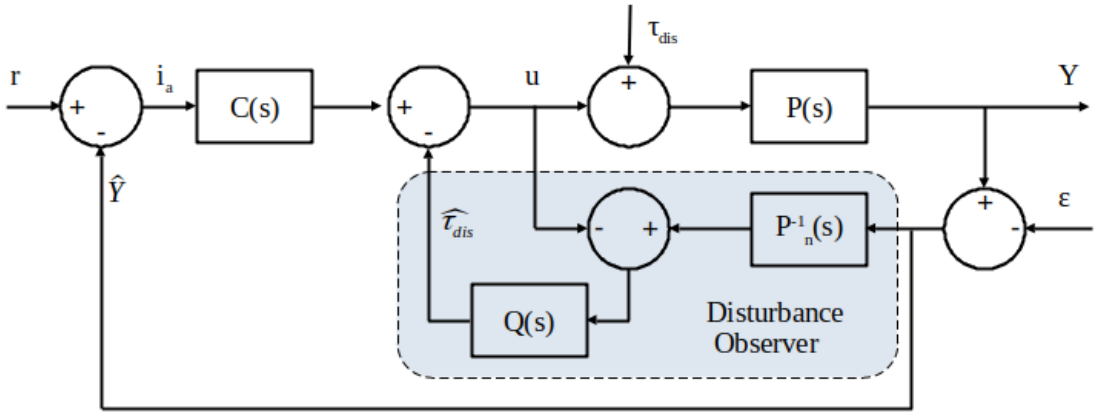

Fig. 2.1: A disturbance observer model combined with a controller

TABLE 2.1: NOMENCLATURE OF TERMS

Parameter	Description
$P_n(S), P(S)$	Models of nominal and real plants
$Y, \hat{Y}$	Output and Measured output
$C(S)$	Controller for the outer loop
$Q(S)$	Low pass filter of DoB
r, e	Reference signal for the controller and measurement noise
$d_{dis}, \hat{d}_{dis}$	Disturbance and Estimated disturbance
$u, \hat{u}_n$	Plant input, estimated nominal plant input
ζ	Measurement noise

$$H_{uy} = \frac{y}{u} = \frac{PP_n}{Q(P - P_n) + P_n} \tag{2.1}$$

$$H_{dy} = \frac{y}{d} = \frac{PP_n(1 - Q)}{Q(P - P_n) + P_n} \tag{2.2}$$

$$H_{\zeta y} = \frac{y}{\zeta} = \frac{PQ}{Q(P - P_n) + P_n} \tag{2.3}$$

The transfer function, sensitive function, and co-sensitive function are represented by the Equations 2.1, 2.2, and 2.3 respectively. By assuming that the nominal plant and the actual plant are similar, these equations can be further simplified. The simplified equations are shown in Equations 2.4, 2.5, and 2.6.

$$H_{uy} = P \tag{2.4}$$

$$H_{dy} = P(1 - Q) \tag{2.5}$$

$$H_{\zeta y} = Q \tag{2.6}$$

According to the derived equations, when the nominal and actual plant modals are identical, the existence of the inner loop is not noticeable to the outer loop. This separation of the two loops allows them to be individually designed and adjusted, which is referred to as the separation principle in control systems.

Equations 2.5, and 2.6's sensitive and co-sensitive functions delineate the influence of both disturbance and measurement noise, correspondingly, on the achievement of performance goals. Furthermore, Equations 2.5, and 2.6 also explain that the effects of uncertain dynamics can be avoided with a carefully designed filter Q. Following Equation 2.4, the filter must be unity to minimize the effect of disturbances. Additionally, the filter must have zero values at higher frequencies to reduce the impact of noise. This implies that the filter required for integration should be a low pass filter.

2.3 Disturbance Observer (DoB) integrated to a DC Motor

Figure 2.2 depicts the electrical portrayal of a DC motor.. In Figure 2.2, L stands for armature inductance, i_a denotes the armature current, v_a denotes the voltage difference between the motor armature, and R represents the armature resistance.

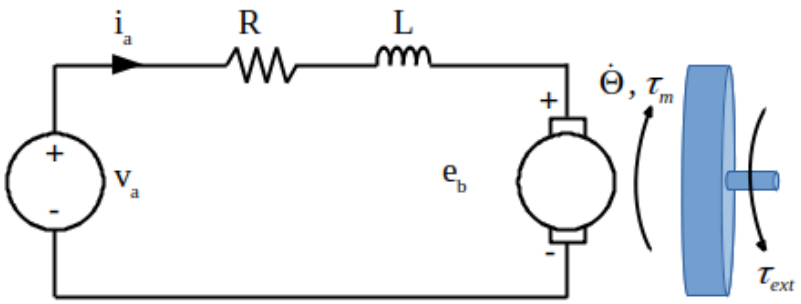

Fig. 2.2: Electrical representation of a DC motor

The overall mechanical torque generated by the DC motor is expressed by τ_m. Taking the torque constant as K_t, the τ_m can be derived as in Equation 2.7.

$$\tau_m = K_t i_a \tag{2.7}$$

Motor torque τ_m can also be expressed as a sum of torques as in Equation 2.8.

$$\tau_m = J\frac{d\dot{\theta}}{dt} + B\dot{\theta} + \tau_{fric} + \tau_{int} + \tau_{ext} \tag{2.8}$$

Where,

J	Inertia of the DC motor
$B\dot{\theta}$	Viscous friction of the DC motor
τ_{fric}	Torque caused by static friction
τ_{ext}	Reaction torque caused due to external contacts
τ_{int}	Interactive torque (This is zero for single DOF systems)

The Equation 2.8 can be re-written in the laplace domain as in the Equation 2.9.

$$\dot{\theta(s)} = \frac{\tau_m + [B\dot{\theta} + \tau_{fric} + \tau_{int} + \tau_{ext}]}{Js} \tag{2.9}$$

The acceleration based block diagram of a DC motor is derived referencing the Equation 2.7 and Equation 2.9, as shown in Figure 2.3.

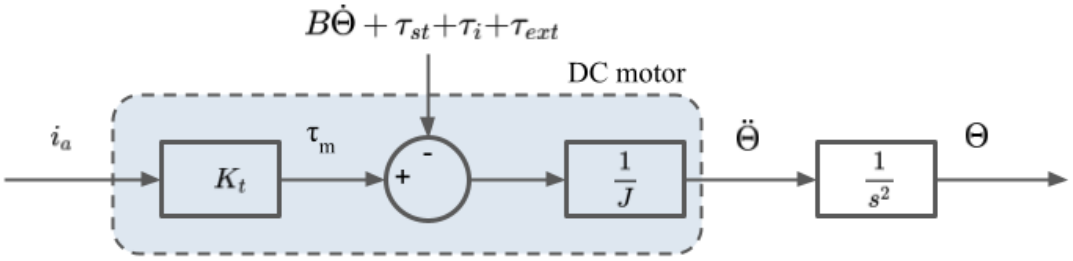

Fig. 2.3: Acceleration based block diagram of a DC motor

2.4 Acceleration based Disturbance Observer Model

Implementing disturbance observers requires first estimating the nominal plant. As a result, performing an accurate system parameter estimation process is required.

Parameter inertia and torque constant are two significant parameters among the parameters to be estimated.These can be subjected to variations and estimation errors. Assuming that $\triangle_J$ and $\triangle_K$ are inertial and torque constant estimation errors, Equation 2.10 and Equation 2.11 can be derived.

$$J = J_n + \triangle J \tag{2.10}$$

$$K_t = K_{tn} + \triangle K_t \tag{2.11}$$

Equation 2.12 can be derived by substituting Equation 2.10 and Equation 2.11 equations for the Equation 2.9.

$$J_n\ddot{\theta} = K_{tn}I_a - [\tau_{fric} + \tau_{init} + \tau_{ext} + B\dot{\theta} + \triangle J\ddot{\theta} - \triangle K_t I_a] \tag{2.12}$$

The motor disturbance is formulated by the sum of the terms in parentheses, and it is given in Equation 2.13.

$$\hat{\tau_{dis}} = \tau_{fric} + \tau_{int} + \tau_{ext} + B\dot{\theta} + \triangle J\ddot{\theta} - \triangle K_t I_a \tag{2.13}$$

Equation 2.14 is derived by rearranging the Equation 2.12 and Equation 2.13.

$$\hat{\tau_{dis}} = K_{tn}I_a - J_n\ddot{\theta} \tag{2.14}$$

If the armature current and rotor acceleration are known, the total impedance of the motor can be estimated. This is further illustrated in Figure 2.4, and is referred to as the acceleration based DoB model in the control literature.

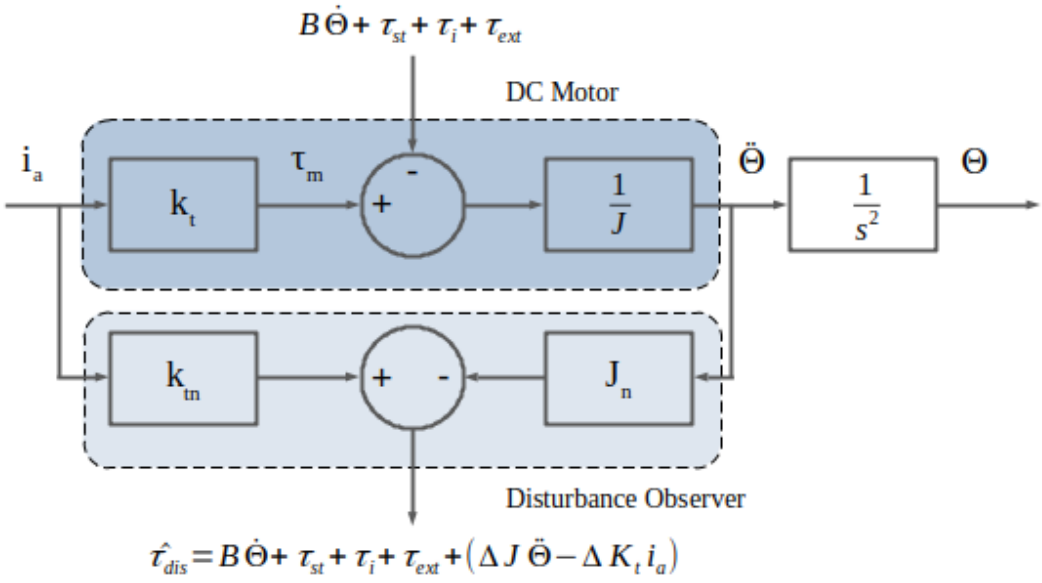

Fig. 2.4: Acceleration based Disturbance Observer

2.5 Modified DoB Model

However, rotary encoders are unable to measure the rotational acceleration directly. This is estimated by taking the twice derivative of the rotational displacement in the time domain. This adds a higher degree of noise to the estimate. Therefore, a low pass filter is added after the disturbance observer estimation. The deduced disturbance

result is then expressed in Equation 2.15. Here, g_{dis} stands for the cut off frequency of the disturbance observer's low pass filter.

$$\hat{\tau_{dis}} = \frac{g_{dis}}{s + g_{dis}}(K_{tn} I_a - J_n \ddot{\theta}) \tag{2.15}$$

As in the equation Equation 2.16, the Equation 2.15 equation can be re-written from angular velocity.

$$\hat{\tau_{dis}} = \frac{g_{dis}}{s + g_{dis}} K_{tn} I_a - \frac{s}{s + g_{dis}} g_{dis} J_n \ddot{\theta} \tag{2.16}$$

Equation 2.17 can be derived by further rearranging the Equation 2.16 equation.

$$\hat{\tau_{dis}} = \frac{g_{dis}}{s + g_{dis}}(K_{tn} I_a + g_{dis} J_n \dot{\theta}) - g_{dis} J_n \dot{\theta} \tag{2.17}$$

The resulting modified DoB model is obtained and is depicted in Figure 2.5.

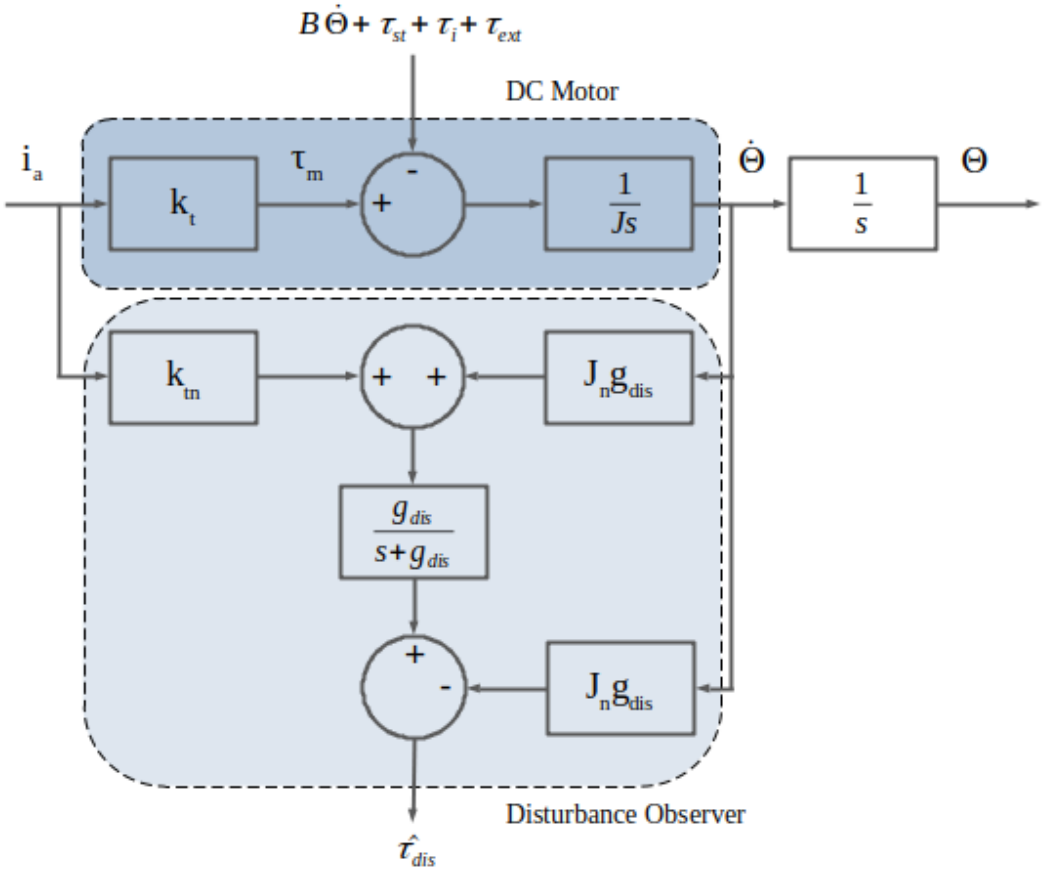

Fig. 2.5: Modified DoB Model

The estimated disturbance torque includes the external torque acting on the motor. By knowing the system parameters, it is possible to estimate the unknown external torque by further modifying the DoB modal.

2.6 Reaction Torque Observer (RTOB)

In force control applications, a wider bandwidth of force measurements can be obtained using RTOB instead of a traditional force sensor. The measuring bandwidth can be controlled by changing the cutoff frequency value and the controller sampling time.

The mathematical model of RTOB can be developed in the same way as the Equation 2.18, subjecting the external torque to the Equation 2.18. g_{RTOB} is the low pass filter cut off frequency in reaction torque observer. The block diagram of the reaction torque observer is presented on Figure 2.6.

$$\hat{\tau_{ext}} = [K_{tn}I_a + J_n g_{RTOB}\dot{\theta} - (\tau_{fric} + B\dot{\theta} + \tau_{int} + \triangle J\ddot{\theta} - \triangle K_t I_a)]\frac{g_{RTOB}}{s + g_{RTOB}} - J_n g_{RTOB}\dot{\theta} \tag{2.18}$$

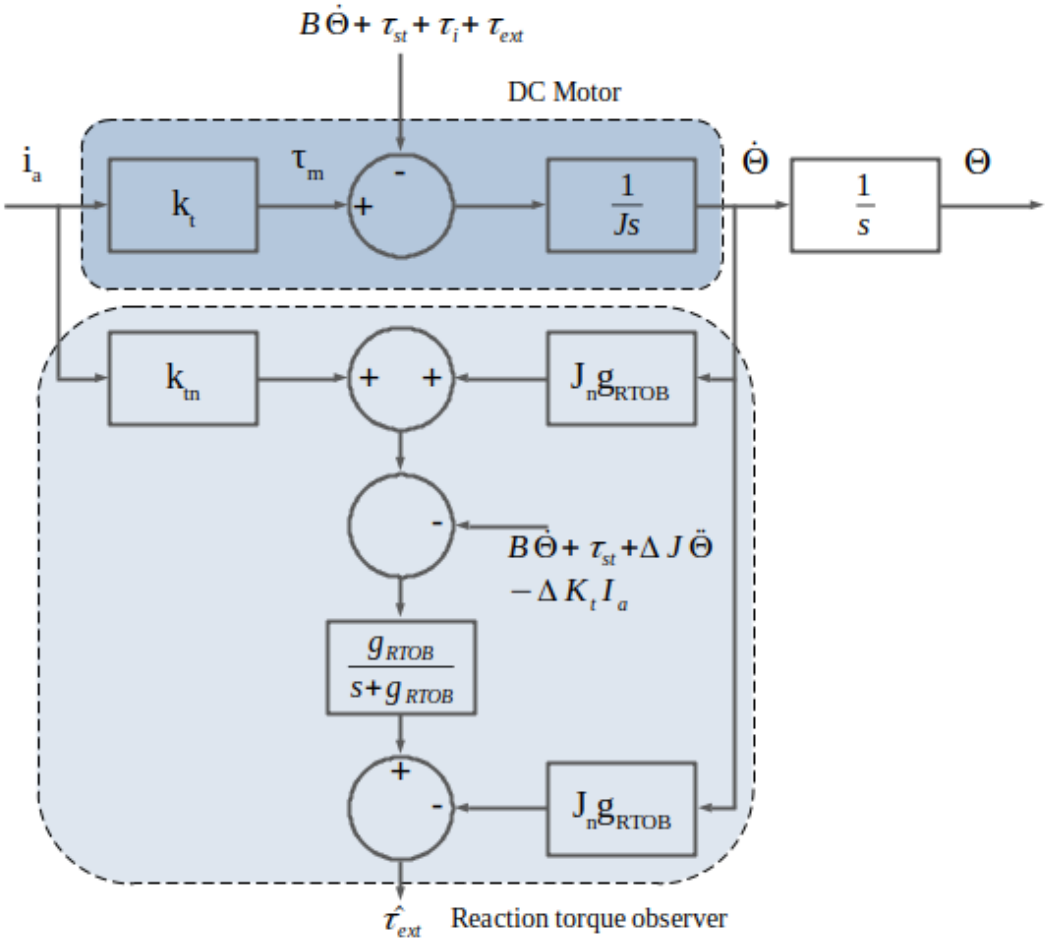

Fig. 2.6: Reaction Torque Observer as a force sensor

CHAPTER 3

AN ITERATIVE APPROACH FOR PARAMETER ESTIMATION IN DC MOTOR BASED MOTION SYSTEMS

3.1 Introduction

Parameter estimation of small-scale DC motors is a challenging task compared to its large-scale counterparts. This chapter has proposed a novel technique to estimate parameters based on a disturbance observer and an optimization algorithm for DC motor-based motion systems. A simplified but accurate cost function is proposed for the disturbance observer-based model. The moment of inertia, coefficient of viscous friction and static friction are estimated and compared with actual parameters. Simulations were carried out to justify the approach.

3.2 Modeling

Assuming the system model depicted in Figure 2.5, the estimated disturbance torque can be reduced to the Equation 3.1 because the system is a 1 dof system.

$$\hat{\tau_{dis}} = \tau_{fric} + \tau_{ext} + B\dot{\theta} + \triangle J\ddot{\theta} - \triangle K_t i_a \tag{3.1}$$

3.3 Linear Regression Model

This section is focused on deriving a linear regression model that relates the system parameters to the DoB estimation. Furthermore, the problem of system parameter estimation has also been reformulated as a problem of parameter estimation in a linear regression model.

The general form of a multi-variable linear regression model can be presented as Equation 3.2 [24].

$$y(k) = a_0x_0(k) + a_1x_1(k) + a_2x_2(k) + ... + a_nx_n(k) \tag{3.2}$$

The vector form of the equation Equation 3.2 can be expressed as the Equation 3.3.

$$y(k) = X(k)A \tag{3.3}$$

where,

$$X(k) = \begin{bmatrix} x_0(k) & x_1(k) & x_2(k) & ... & x_n(k) \end{bmatrix}$$
$$A^T = \begin{bmatrix} a_0 & a_1 & a_2 & ... & a_n \end{bmatrix}$$

$y(k)$	Measured output
$X(k)$	Vector of measurable quantities
A	Vector of unknown parameters

Here, k represents the data point at time kdt, dt is the sampling time.

3.4 Problem formulation

Generally, the torque constant of a motor is constant over time compared to other motor parameters. If the environment exerts no torque, it is possible to simplify the derived motor model by ignoring changes in the motor constant. Hence, the equation Equation 3.1 can be reduced to the equation Equation 3.4.

$$\hat{\tau_{dis}} = \tau_{fric} + B\dot{\theta} + \triangle J\ddot{\theta} - \triangle K_t I_a \tag{3.4}$$

Angular acceleration and angular velocity are known parameters. If the parameters $\triangle J$, B and τ_{fric} are known, the disturbance observer estimate can be achieved. The aim of this approach is to fit these unknown coefficients in such a way that the disturbance observer output coincides with the prediction of the model represented in equation Equation 3.4.

For the ease of formulation, equation Equation 3.4 is rearranged as equation Equation 3.5.

$$\hat{\tau_{dis}}^e = \begin{bmatrix} 1 & \dot{\theta(k)} & \ddot{\theta} \end{bmatrix} \begin{bmatrix} \tau_{fric} \\ B \\ \triangle J \end{bmatrix} \tag{3.5}$$

Note that Equation 3.5 is in the form described in Equation 3.3, Where,

$$X(k) = \begin{bmatrix} 1 & \dot{\theta(k)} & \ddot{\theta(k)} \end{bmatrix}$$
$$A^T = \begin{bmatrix} \tau_{fric} & B & \triangle J \end{bmatrix}$$

Therefore, it is clear that the system parameter estimation can be achieved by parameter estimation of the linear regression model presented in Equation 3.5.

3.5 Objective/ Loss function

The least square error approach is simple yet a powerful numerical method in mathematics for optimization problems. The unknown variables of the model represented in Equation 3.3 can be computed using an iterative approach by minimizing the square error $E(A_i)$ which is formulated in Equation 3.6. Here, i^{th} iteration of the optimization process is represented by the letter i. The square error function, which is described in Equations 3.6 and Equation 3.7, is the objective function or the loss function. It will be optimized in the next section to compute the unknown parameter matrix A.

$$E(A_i) = \frac{1}{2m}\sum_{k=1}^{m}(\tau_{\hat{dis},k} - \tau_{\hat{dis},k}^{e})^2 \tag{3.6}$$

Substituting Equation 3.2 to Equation 3.6, Equation 3.6 is derived.

$$E(A_i) = \frac{1}{2m}\sum_{k=1}^{m}(\tau_{\hat{dis},k} - (a_0x_0(k) + a_1x_1(k) + a_2x_2(k) + ... + a_nx_n(k)))^2 \tag{3.7}$$

Here, m is the number of data samples and $x_{1,k}$ is the k^{th} reading of angular velocity / $\dot{\theta(k)}$ used in the estimation process.

3.6 Model Fitting for parameter estimation

The system parameter estimation of a DC motor can be obtained by solving the regression model that was derived in the previous section. Using that regression model, a novel method for parameter estimation is implemented.

3.6.1 Newton Raphson Algorithm (NRA) for Least Square Error estimation

The pre-defined regression problem is optimized to find the best possible corresponding solution. Usually, this is accomplished through a series of iterations. The choice of optimization algorithm is made after taking into account a number of variables, including the linearity of the task, influencing constraints, and the quantity of unknowable parameters.

The Leven-berg-Marquardt method, steepest descent, and gradient descent are some of the most popular optimization algorithms. However, they have a number of disadvantages, including high noise sensitivity, computational costs, and solutions that are not the best local minimum.

A novel system parameter estimation is presented in this section. The cost function is optimized using Newton Raphson Algorithm. The shortcomings of the prior

optimization algorithm are overcome by the one chosen here. Furthermore, rapid convergence can be achieved. As a result, NRA permits the use of a parameter estimation method that is appropriate for real-time applications.

The NRA is an effective iterative method for resolving algebraic problems. An ideal solution can be obtained from an initial guess by refining the guess up until a tolerable error measure is attained. A series of second order Taylor expansions of $E(A_i)$ around the iterates are used to calculate the increment. Equations 3.8 [25] can be used to express the second order Taylor expansion of $E(A_i)$ around A_i.

$$E(A_i + \triangle A) \approx E(A_i) + \nabla E(A_i)\triangle A + \frac{1}{2}\nabla^2 E(A_i)(\triangle A)^2 \tag{3.8}$$

The definition of the subsequent iteration, A_{i+1}, aims to minimize the quadratic approximation of $\triangle A$. The iterate A_{i+1} is then determined using Equations 3.9.

$$E(A_{i+1}) = E(A_i) + \triangle A \tag{3.9}$$

A minimum exists because the quadratic approximation is a convex function of $\triangle A$. By setting the derivative to zero as shown in equations 3.10, this minimum is attained.

$$\frac{d}{d(\triangle A)}(E(A_i) + \nabla E(A_i)\triangle A + \frac{1}{2}\nabla^2 E(A_i)(\triangle A)^2) = 0 \tag{3.10}$$

Simplifying Equations 3.10, Equations 3.11 can be derived.

$$\nabla A_i + \nabla^2 A_i(\triangle A) = 0 \tag{3.11}$$

As a result, the recursive term in NRA can be derived as in Equations 3.12.

$$A_{i+1} = A_i - \nabla^2 A^{-1} \triangle A \tag{3.12}$$

The gradient matrix of A_i is represented by $\triangle A$, and $\nabla^2 A$ is the hessian matrix of A_i. The equations 3.13 and 3.14 can be used to describe these two matrices.

$$\nabla^2 A_i = \begin{bmatrix} \frac{\partial^2 E(A_i)}{\partial a_0^2} & \frac{\partial^2 E(A_i)}{\partial a_0 \partial a_1} & \frac{\partial^2 E(A_i)}{\partial a_0 \partial a_2} \\ \frac{\partial^2 E(A_i)}{\partial a_1 \partial a_0} & \frac{\partial^2 E(A_i)}{\partial a_1^2} & \frac{\partial^2 E(A_i)}{\partial a_1 \partial a_2} \\ \frac{\partial^2 E(A_i)}{\partial a_2 \partial a_0} & \frac{\partial^2 E(A_i)}{\partial a_2 \partial a_1} & \frac{\partial^2 E(A_i)}{\partial a_2^2} \end{bmatrix} = \frac{1}{m} X^T * X \tag{3.13}$$

$$\nabla A_i = \frac{1}{m} \begin{bmatrix} \sum_{k=1}^{m} (\tau_{\hat{dis},k} - \sum_{j=0}^{2} a_j x_{j,k}) x_{1,k} \\ \sum_{k=1}^{m} (\tau_{\hat{dis},k} - \sum_{j=0}^{2} a_j x_{j,k}) x_{2,k} \\ \sum_{k=1}^{m} (\tau_{\hat{dis},k} - \sum_{j=0}^{2} a_j x_{j,k}) x_{3,k} \end{bmatrix} \tag{3.14}$$

Where X is the matrix with the dimensions m by 3 that holds all the measured data. Figure 3.1 provides an overview of the algorithm by showing how to estimate a

DC motor's system parameters using NRA.

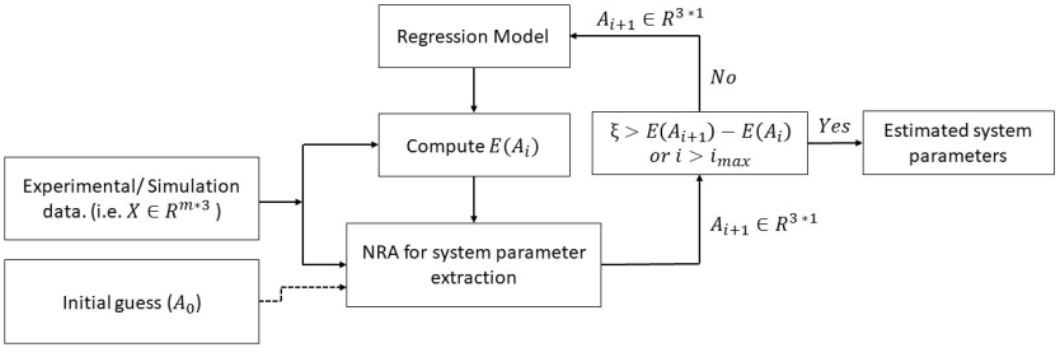

Fig. 3.1: DC motor parameter estimation using Newton Raphson Algorithm (NRA)

3.7 Simulations

Computer simulations have been carried out with the aid of a programming platform to show the effectiveness and viability of the proposed technique. For the purposes of the simulation, a typical DC motor controlled by an established PID-based velocity controller, as shown in Figure 3.3, has been taken into account. Table 3.1 includes a list of the setup's system requirements and specifications for the simulated DC motor

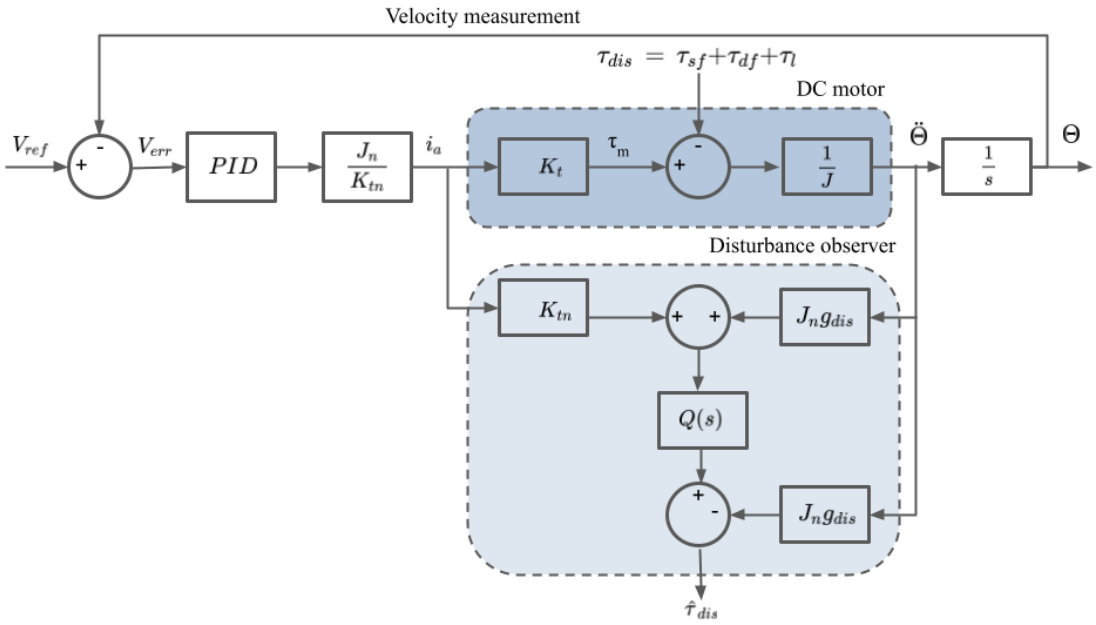

Fig. 3.2: Model of a DC motor integrated with a velocity controller and a DoB

TABLE 3.1: SPECIFICATIONS OF THE SIMULATED DC MOTOR AND THE CONTROLLER

Specifications	Values
K_t	0.135 [Nm/A]
J	0.000072 [Nms^2/rad]
B	0.02045 [Nms/rad]
τ_{fric}	0.0182 [Nm]
K_p	5500
dt	200 [μs]

During the simulation, it was assumed that all DC motor parameters would remain constant. Unstructured uncertainties such as changes in environmental conditions, hysteresis, and saturation were ignored. The simulation data was produced by a DC motor with a DoB integrated. For the parameter estimation process, armature current, angular velocity, angular acceleration, and the DoB estimation were recorded. The accuracy of the suggested method has been assessed using a random velocity reference, which is shown in Figure 3.3.

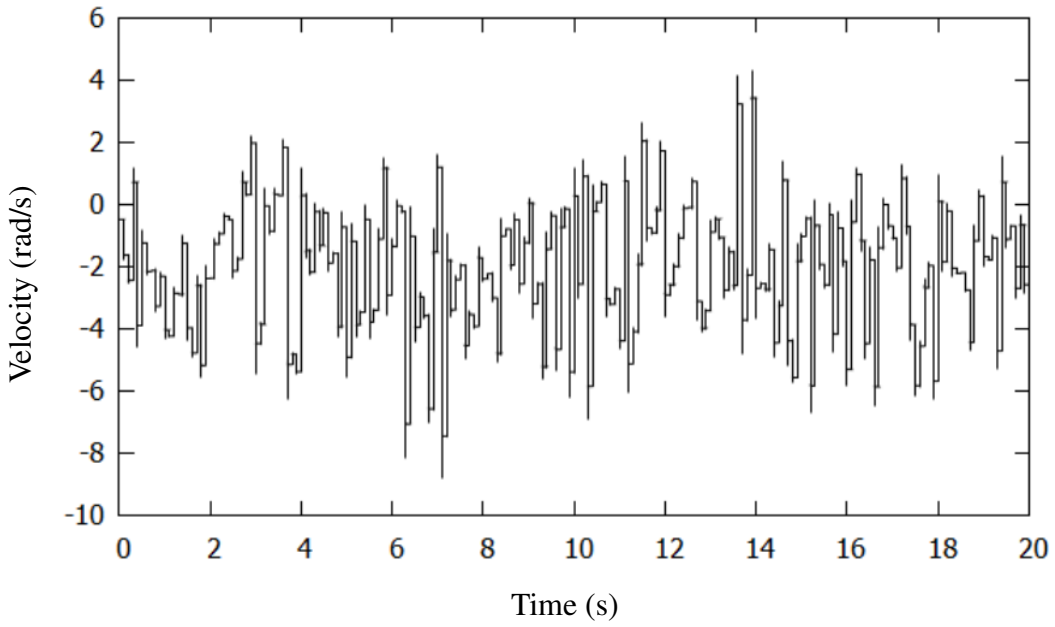

Fig. 3.3: Velocity Reference to the Controller

For the purpose of evaluating the proposed method's ability to achieve convergence, simulations were run under two scenarios with various numbers of unknown parameters. In each simulation, NRA was performed on recorded data for 5 iterations.

The variations of inertia ($\triangle J$) were set to zero in the first simulation scenario.

Only static friction and viscous friction coefficient were taken into account during the testing. Equations 3.15 represents the modified model equation that was applied in this simulation.

$$\hat{\tau_{dis}}(k) = B\dot{\theta}(k) + \tau_{sf} \tag{3.15}$$

In Figures 3.4 to 3.8 the outcomes are displayed. The objective function behavior is represented by the 3D and 2D contour spaces in Figures 3.4, 3.5. These graphs demonstrate the global minima of the objective function and the route taken by NRA to reach it. The convergence of the objective function depicted in Equations 3.6 is shown in Figure 3.6. The appropriateness of the NRA for parameter estimation has been established because the objective function quickly attained a stable value. The estimated system parameters are shown to converge as the number of iterations rises in Figure 3.7 and Figure 3.8. The estimated values from the simulation match the actual values, which are listed in Table 3.2.

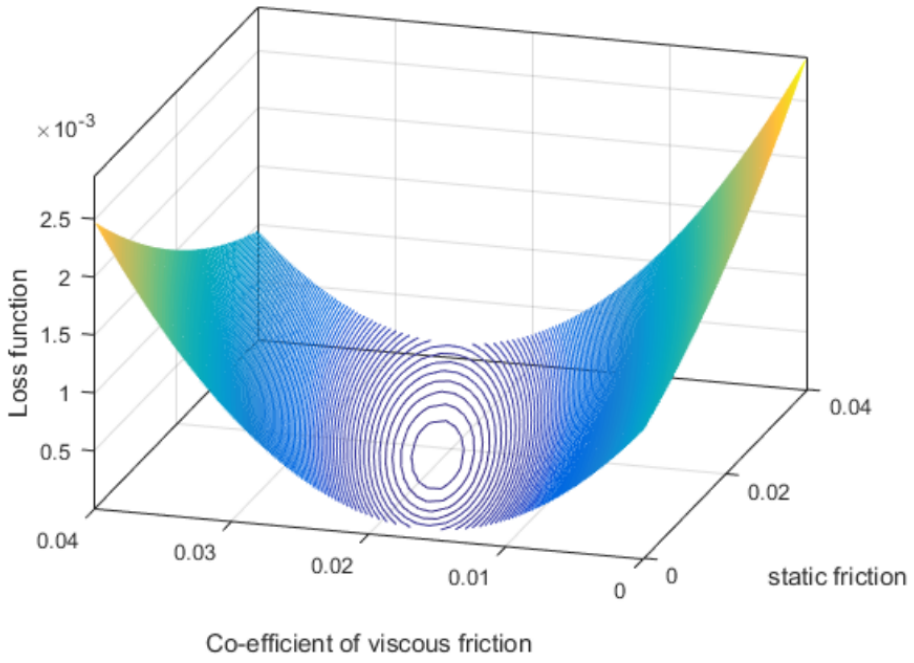

Fig. 3.4: 3D contour space of loss function

In the second simulation variation of inertia ($\triangle J$) is also considered. The model equation is therefore expressed as Equation 3.4. The convergence of the loss function, static friction, estimated coefficient of viscous friction, and variation of inertia against the number of iterations are shown in Figures 3.9, 3.10, 3.11, and 3.12. Despite the number of unidentified parameters, the NRA's estimation of the parameters was very accurate. In Table 3.2, a comparison of estimated and actual values is presented.

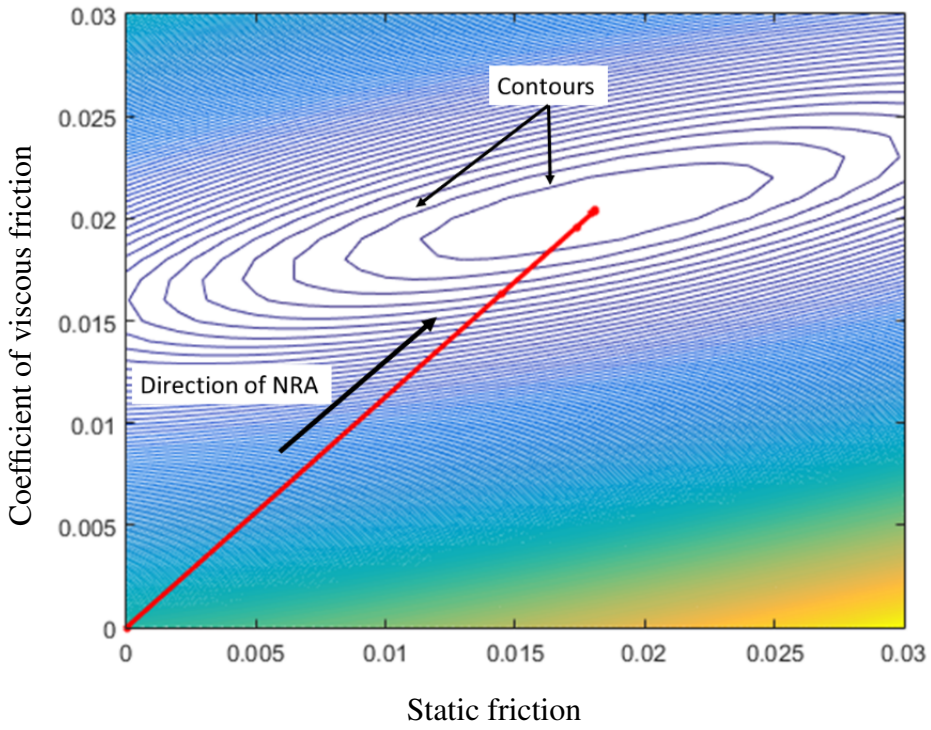

Fig. 3.5: Path of NRA in contour space

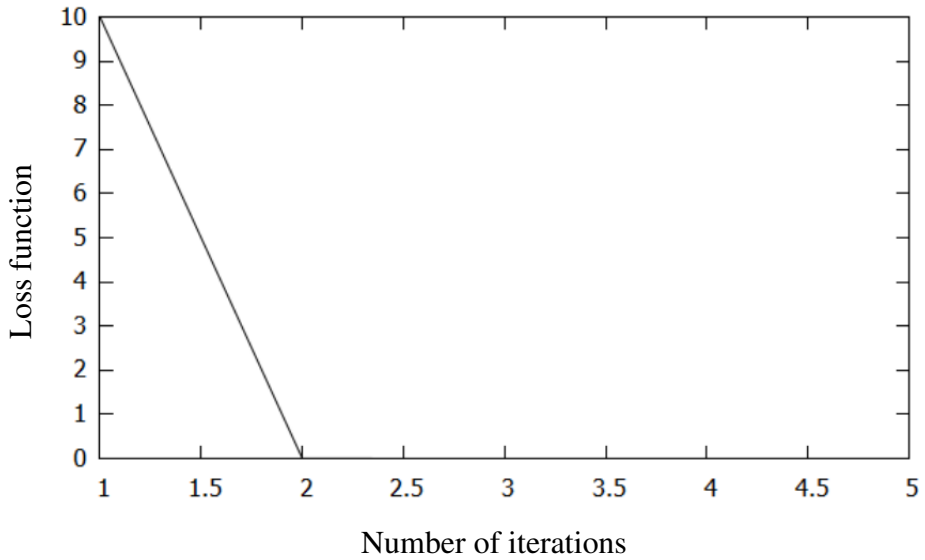

Fig. 3.6: Test 1 - Convergence of E(A)

3.8 Conclusion

In this study, a novel method for estimating DC motor parameters has been presented. Traditional methods of DC motor parameter estimation have a low level of accuracy in small scale applications. To perform small scale motion applications, however, accu-

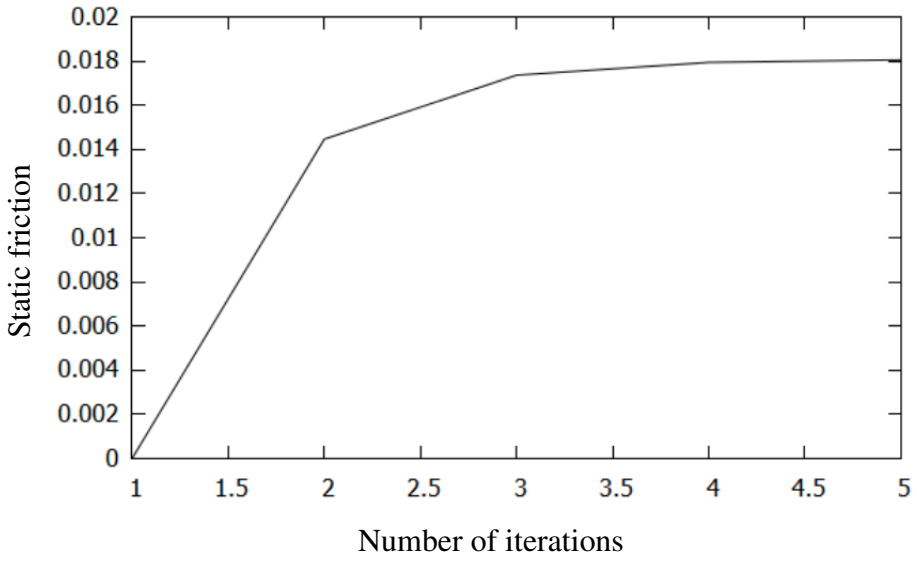

Fig. 3.7: Test 1 - Convergence of static friction parameter

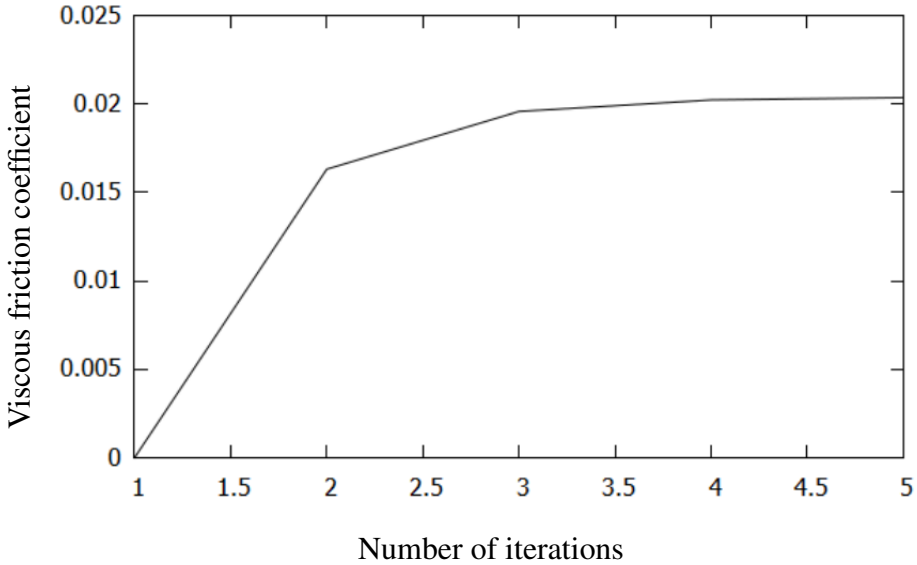

Fig. 3.8: Test 1 - Convergence of viscous friction co efficient

rate estimation of DC motor parameters is essential. The disturbance observer's (DoB) predictions of the DC motor serve as the foundation for this method. This study has developed a regression model that connects system parameters and motor parameters to the DoB estimation. The derived regression model can be optimized to estimate the motor parameters.

Due to its accuracy and speed, the Newton Rapshson algorithm has been chosen over other optimization algorithms like gradient descent to optimize the derived regression model. In the simulations section, the feasibility of the suggested method was verified and contrasted.

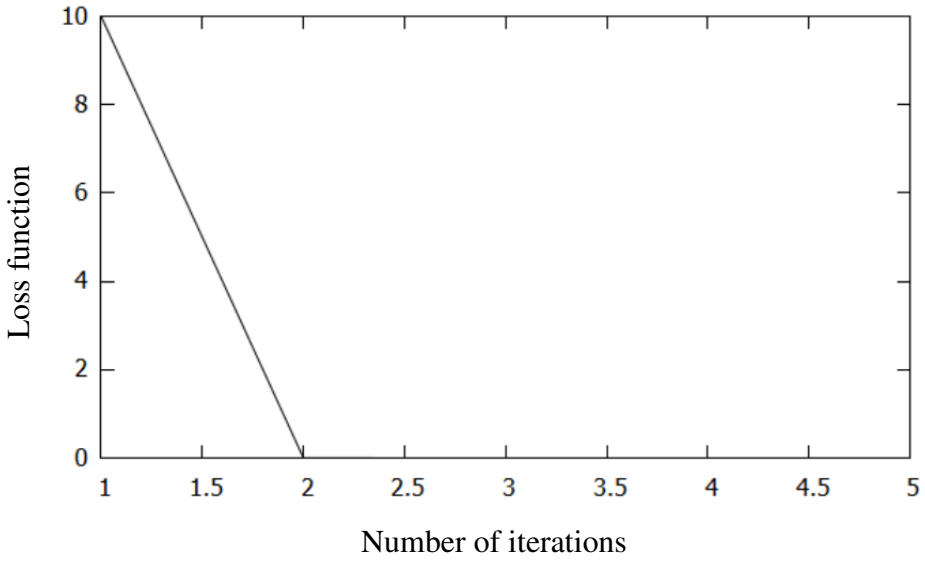

Fig. 3.9: Test 2 - Convergence of E(A)

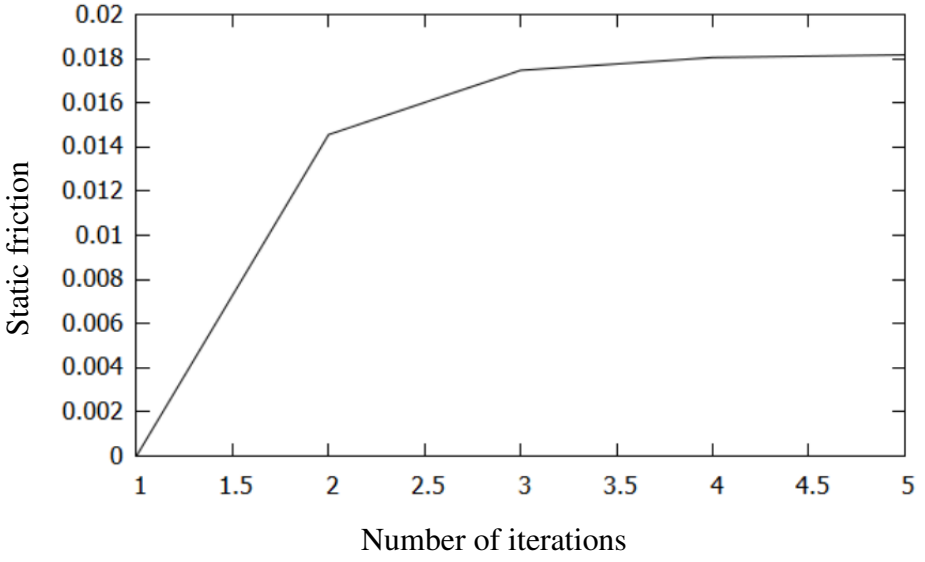

Fig. 3.10: Test 2 - Convergence of static friction parameter

TABLE 3.2: TEST RESULTS

Parameter	Actual Value	Estimated Value
Test - 1		
τ_{sf}	0.0182 [Nm/A]	0.0181 [Nm]
B	0.02045 [Nms/rad]	0.0204 [Nms/rad]
Test - 2		
τ_{sf}	0.0182 [Nm/A]	0.0181 [Nm]
B	0.02045 [Nms/rad]	0.0204 [Nms/rad]
$\triangle J$	0.00002 [Nms^2/rad]	0.0000159 [Nms^2/rad]

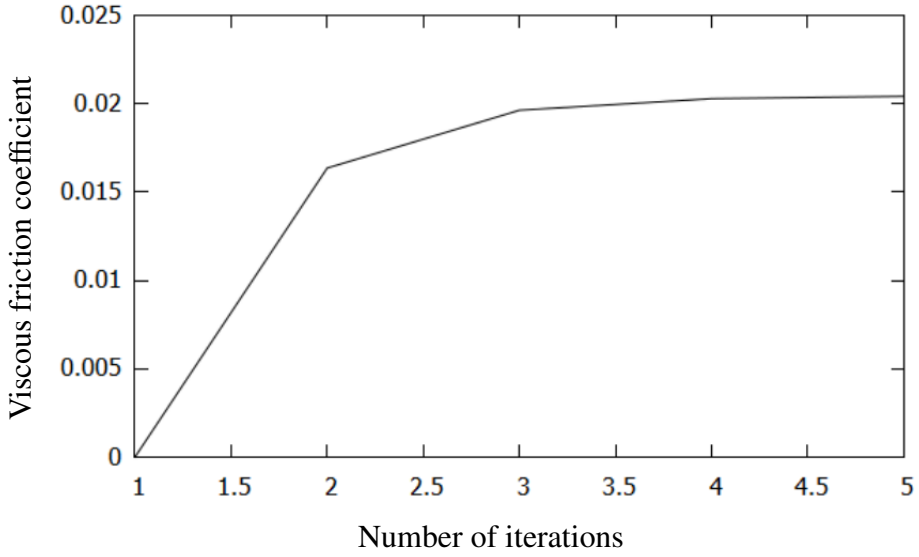

Fig. 3.11: Test 2 - Convergence of viscous friction co efficient

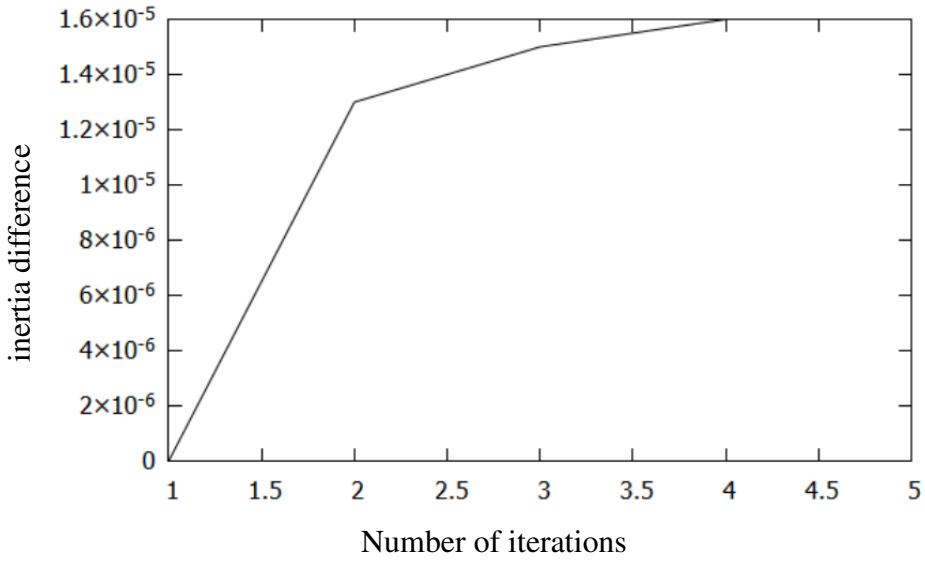

Fig. 3.12: Test 2 - Convergence of inertia difference

CHAPTER 4

USING DISTURBANCE OBSERVERS TO SUPPRESS VIBRATIONS IN FORCE CONTROLLERS

A serious problem brought on by vibrations is the performance degradation of motion control systems like force, position, and velocity controllers. Control engineers have therefore created a variety of techniques to reduce vibrations in motion control systems.

Consider Figure 4.1, which depicts an actuator that utilizes a motor to apply a constant force to a stationary object. The actuator axis is subjected to an external vibration torque of τ_v. The end of the actuator experiences positional vibration due to the presence of vibration torque τ_v. In light of this scenario, Newton's third law can be used to derive Equation 4.1.

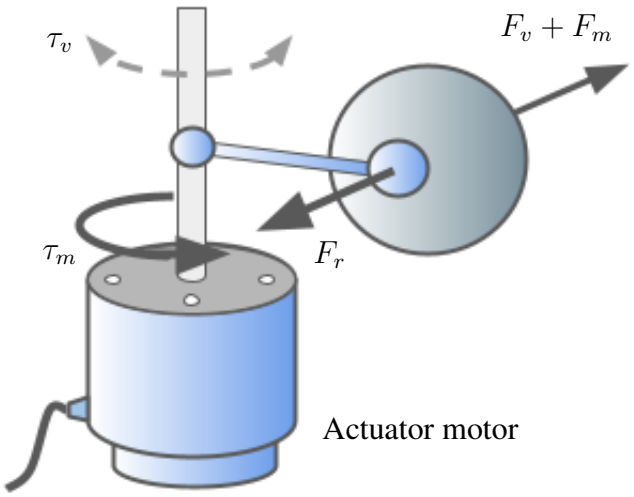

Fig. 4.1: External vibrations on force system

$$F_r = F_m + F_v \tag{4.1}$$

where,

F_r Reaction force
F_v Force acting on the external environment(object) due to torsional vibration τ_v
F_m Force acting on the external environment(object) due to the motor torque τ_m

In a conventional force controller, F_m is a constant. Therefore, the reaction force, F_r on the external environment changes along with the vibration force F_v, as shown

by Equation 4.1. In simpler terms, the object can sense fluctuations from outside. The object won't experience vibrations if F_r is maintained constant in spite of F_v fluctuations. This reaction force is not measurable because of sensor limitations. Therefore, if conventional force controllers are employed, reaction force control is ineffective. The position controllers are typically used to achieve vibration suppression. However, the topic of vibration suppression in force controllers is not frequently covered in control literature.

4.1 The impact of vibrations on force control

The usage of force controllers is common in industries like robotics and automation. Figure 4.2 shows the structure of a typical force controller that is susceptible to external vibration. The components of the system include a feedback loop, a force sensor, a force actuator, and a PID controller. To precisely follow the prescribed force/ torque is the aim of a force controller. The measurement of force determines the functional accuracy of a force controller. The force sensor is therefore the most important part of a force controller. The limitations of the force sensor make accurate force controlling difficult. As an illustration, consider the strain gauge, a type of force sensor. Errors and noise are common with strain gauges. They therefore require regular calibrations. Moreover, a strain gauge's limited ability to sense forces and large footprint can have an impact on small-sized systems. The force-measuring bandwidth of strain gauges is constrained, and this has a significant impact on the initial dynamics of the system. A low-pass filter helps lessen a strain gauge's measurement noise. A low pass filter, however, significantly reduces the sensing bandwidth. It is still difficult to employ force sensors for vibration attenuation.

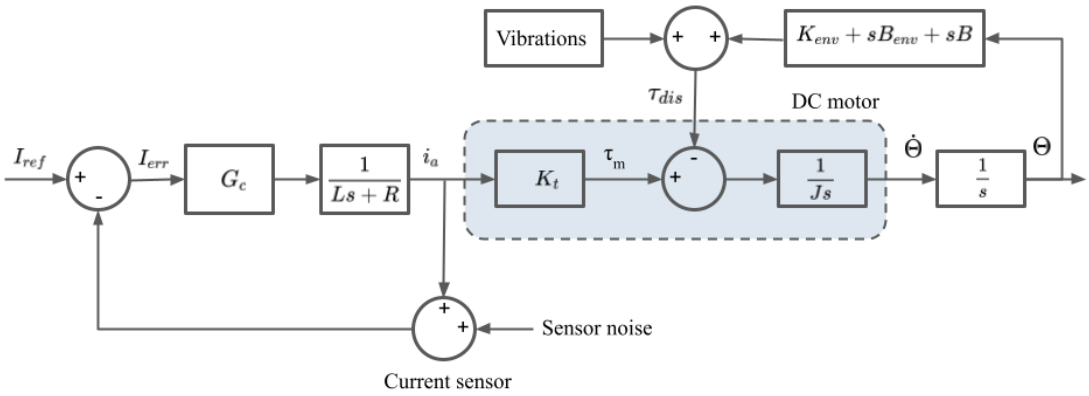

Fig. 4.2: DC motor force actuation using the current control model

Electro-mechanical force actuators predominate. Electro-mechanical force actuators are typically force-controlled by means of current control.

A frequent perturbation that impairs the functioning of force / torque actuators is vibration. As a result, it is necessary to examine the vibration suppression capabilities in torque / force controllers. The following chapter will cover the evaluation of a force/torque controller's performance in the presence of torque vibration, denoted as τ_v.

The force actuator used in the simulations provided in this chapter is powered by a DC motor, as shown in Figure 4.1. Several control structures, such as current controlling, reaction torque observer based force controlling, and reaction torque observer plus disturbance observer (RTOB-DoB) based force controlling, are used to perform them. A sinusoidal axial vibration torque of τ_v is used to represent a sine wave. The simulation settings are presented in Table 5.1, and the object or the environment in contact is modeled as a spring mass damper.

TABLE 4.1: SIMULATION PARAMETERS UTILIZED

Symbol	Parameter	Numerical Value
i_a	Armature current	
I_r	Reference Current	2.0 A
R	Internal resistance of DC motor	0.5 $ohms$
L	DC motor inductance	0.015 H
K_t	Torque constant of the DC motor	0.135 Nm/A
I_{err}	Calculated error in the current	
τ_{dis}	Disturbance torque	
J	Inertia of the DC motor	0.0000072 kgm^2
B	DC motor viscous friction coefficient	0.000905 Nms/rad
τ_v	Vibration torque	$0.5sin(10/\pi * t)Nm$
τ_m	Generated motor torque	
B_{env}	Damping coefficient of environment in contact	0.05 Nms/rad
G_c	Controller transfer function	2500
K_{env}	Spring constant of the environment in contact	80 Nm/rad
τ_s	Reaction torque of the spring	
K_{tn}	Nominal torque constant	0.135 Nm/A
J_n	Nominal inertia of the DC motor	0.000072 kgm^2
τ_{ref}	Reference torque input	0.15 Nm
g_{dis}	DoB LPF's cut off frequency	500 rad/s
K_f	Spring coefficient of force sensor	
g_{RTOB}	RTOB LPF's cut off frequency	2 rad/s

4.2 Traditional torque or force controlling in DC motors

In many controllers, motors serve as torque actuators. Since the armature current and the motor torque that is generated and the actuator force are inversely correlated, the generated motor torque and actuator force can be managed by adjusting the motor current. Thus, a constant armature current can provide a constant motor torque. A DC motor's current control model is shown in Figure 4.2.

In the Laplace domain, Equation 4.2 can be used to explain the transfer function of the traditional force controller based on Figure 4.2.

$$\theta = I_{ref}X + \tau_v Y \tag{4.2}$$

Here Equation 4.3 and 4.4, respectively, express X and Y.

$$X = \frac{G_c K_t}{s(Js + B) + K_{env} + sB_{env}} \tag{4.3}$$

$$Y = \frac{-1}{s(Js + B) + K_{env} + sB_{env}} \tag{4.4}$$

The spring and damper characteristics of the contact environment are indicated here by the letters K_{env} and B_{env}. According to Equation 4.4, the parameters that determine the disturbance attenuation property in a conventional force controller are environmental stiffness and motor inertia.

Figure 4.3 depicts traditional force control using a force sensor. A system with a force sensor can be modeled using two resonant systems. The sensor and actuator are assumed to be two rigid bodies that are connected by a soft structure, which can be visualized as a spring with stiffness denoted by K_s. The two-mass resonant system's dynamic equations can be represented as Equation 4.5, 4.6. When sensor rotation is θ_s and perceived torque is τ_s.

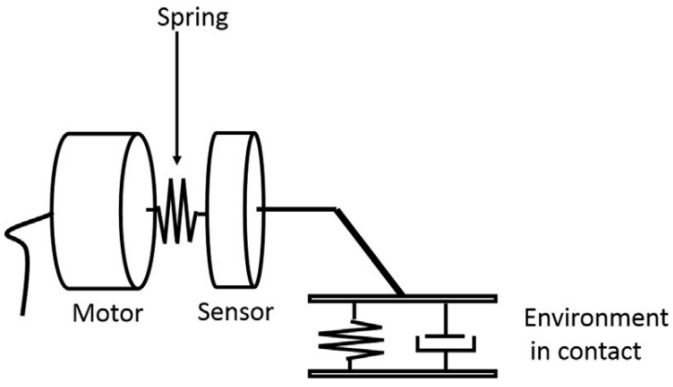

Fig. 4.3: Conventional force controller configuration

$$J_m\ddot{\theta_m} = \tau_m - \tau_s - \tau_{dis} \tag{4.5}$$

$$\tau_s = K_s(\theta_m - \theta_s) \tag{4.6}$$

As a result, modeling the force control system becomes challenging. Moreover, when high-frequency dynamics are present, relative deformation can lead to inaccurate measurements and faults.

4.3 The reaction torque observer as a force sensor

To determine the external forces acting on a motor, a reaction torque observer (RTOB), a derivative of a DoB, is employed. In Figure 4.4, RTOB is shown as a force sensor where a force control system is being affected by a torsional vibration of τ_v.

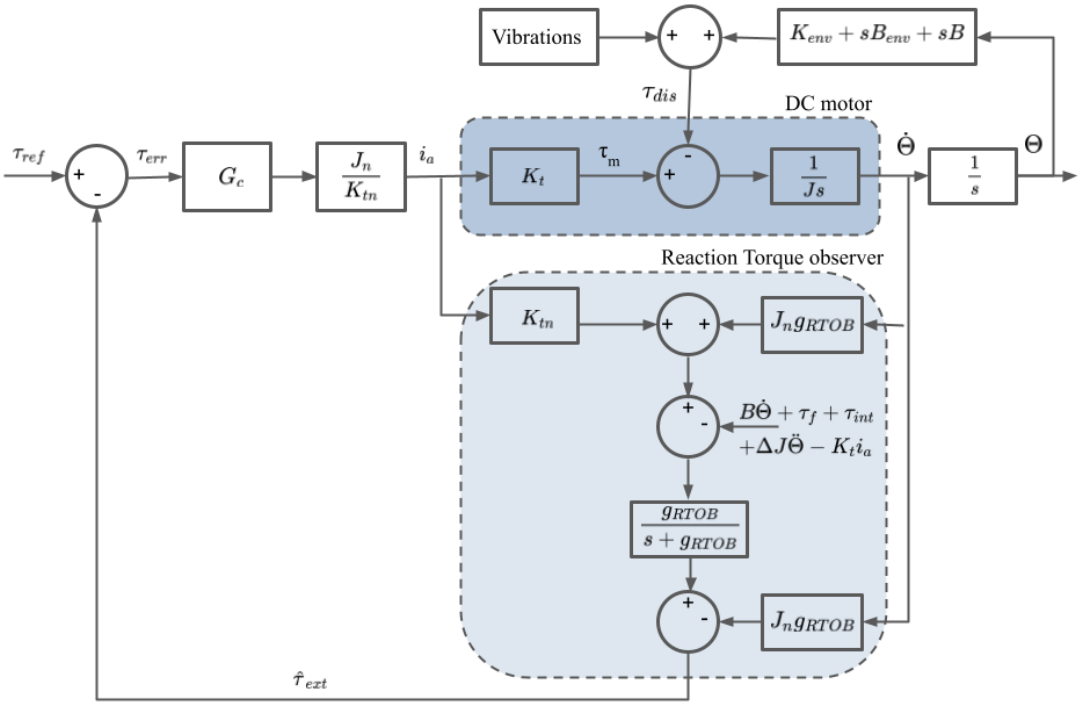

Fig. 4.4: The reaction torque observer as a force sensor

It is necessary to be aware of the parameter variations and frictional components in advance. In Equation 4.7, the transfer function of the force control system with a reaction torque observer is described.

$$\frac{\theta}{\tau_v} = \frac{-a}{s^2 J_n(s + g_{RTOB}) + sB(s + g_{RTOB}) + (K_{env} + sB_{env})a'} \tag{4.7}$$

where,

$$a = g_{RTOB} J_n G_c + s + g_{RTOB} \tag{4.8}$$

4.4 Usage of the DoB to isolate vibration effects

Numerous researchers have tested and verified the disturbance observer based force controller, which can realize a non-changing reaction torque response despite the disturbances [26]. A force controller based on the reaction torque observer and the disturbance observer is shown in Figure 4.5.

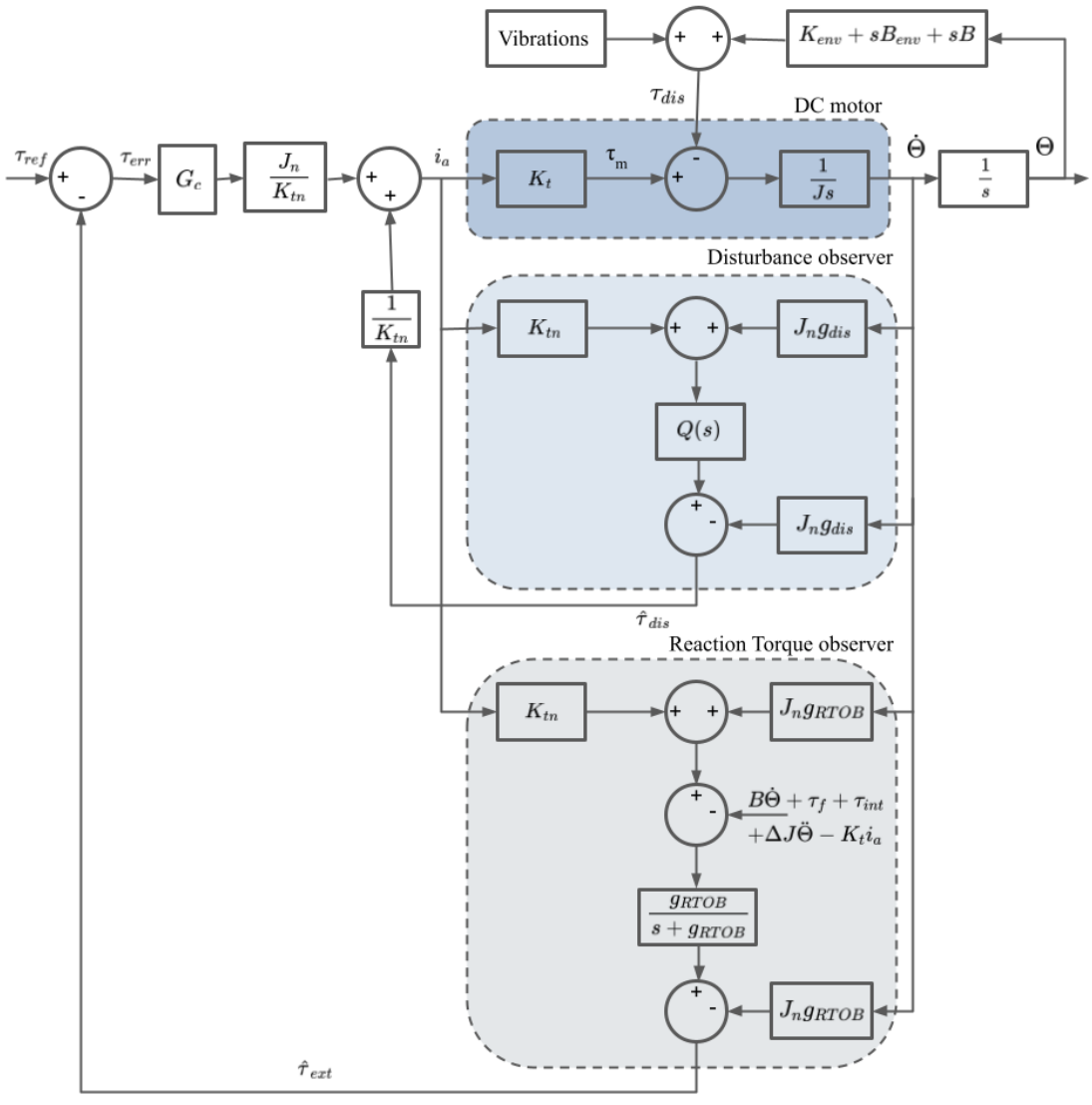

Fig. 4.5: Reaction torque observer plus disturbance observer based force controller

In this setup, the inner loop disturbance observer calculates and accounts for the disturbances while the outer loop RTOB calculates the reaction forces. The cutoff

frequency of the RTOB low-pass filter can be lowered to achieve nonvarying reaction force estimation in force-controlling applications. On the other hand, by increasing the cutoff frequency of the DoB low-pass filter, uncertain vibration disturbances can be precisely estimated from the DoB. As a result, disturbances across a wide bandwidth can be estimated.

Equation 4.9 represents the transfer function of the force controller, which is derived from Figure 4.5.

$$\frac{\theta}{\tau_{dis}} = \frac{-a}{Js^2(s+g_{RTOB})(s+g_{dis}) + (K_{env} + sB_{env})a + s^2B(s+g_{RTOB})a'} \tag{4.9}$$

where,

$$a = s(s+g_{RTOB}) + g_{RTOB}(s+g_{dis})G_cJ_n \tag{4.10}$$

4.5 Simulation results

The three force-controlling techniques; conventional force controller, reaction torque observer based force controller, and reaction torque observer plus disturbance observer based force controller were compared through simulations. A sinusoidal torque disturbance was applied in each of the three instances, after which the positional response was observed. The effectiveness of the controller was evaluated using frequency analysis. The limits of system parameters are revealed by stability analysis.

The controllers in the simulations were given a torque order of 5 Nm. For the force controller based on the current controller, an equal amount of torque-producing current was applied. Therefore, all of the controllers had the same motor torque, τ_m.

In Figure 4.6, the Bode diagrams between the disturbance input and the positional response of these force controllers are depicted.

The disturbance attenuation characteristics of the current-based force controller and the RTOB-based force controller are nearly identical, as shown in Figure 4.6. Additionally, the RTOB-DoB-based force controller has better disturbance suppression capabilities than the other two controllers. According to Figure 4.6(C), the RTOB-DoB-based force controller's disturbance attenuation is improved by the LPF cutoff frequency of the DoB.

The positional response of an RTOB-DoB-based force controller for various DoB's LPF cutoff frequencies is shown in Figure 4.7. By raising the cutoff frequency of the DoB's LPF, better vibration attenuation in positional response can be achieved, as shown in Figure 4.7.

In Figure 4.8, the BODE diagram between the disturbance input and the RTOB output is shown. It can be seen that the force controller based on the RTOB has no way

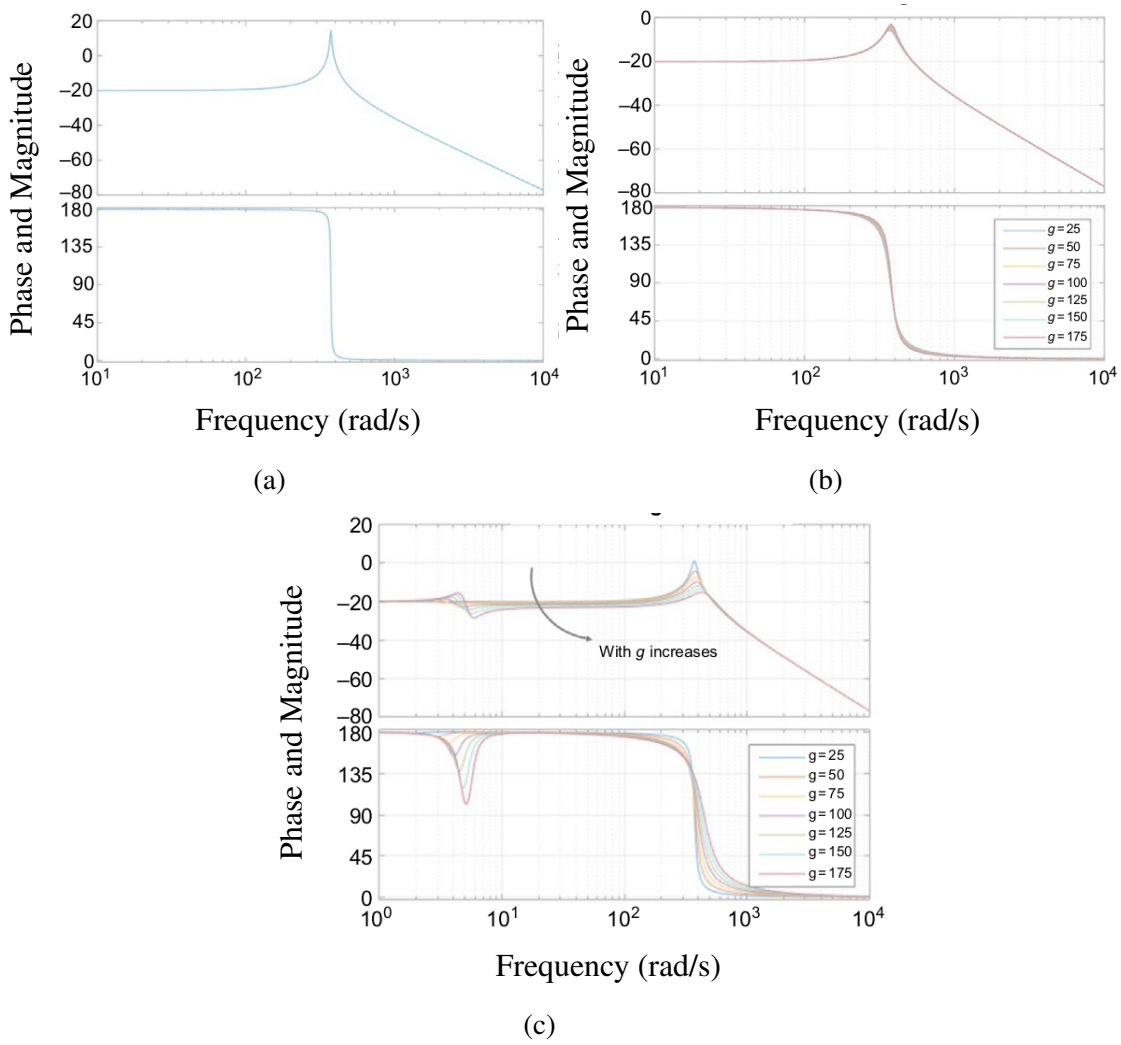

Fig. 4.6: Diagrams depicting the relationship between disturbance input and positional response in force controller models are shown in (A) current controlled mode, (B) RTOB based model with variable RTOB cut-off frequency, and (C) RTOB DoB based model with variable DoB cut-off frequency.

to dampen the disturbances. It is clear from Figure 4.8 that the RTOB's low-pass filter allows the user to choose the bandwidth of the estimated reaction force. By altering the LPF of the RTOB's cutoff frequency, reaction forces over a wider range can be estimated. RTOB has a wider bandwidth as a result than a traditional force sensor.

The bode diagram between the disturbance input and the positional response with the variation of the RTOB cutoff frequency is shown in Figure 4.9.

The positional response to a change in RTOB cutoff frequency is shown in Figure 4.10. According to Figure 4.9 and Figure 4.10, the positional vibration is at its lowest when the RTOB cutoff frequency is lower. In comparison to conventional force controllers, RTOB-DoB-based force controllers can be used to achieve a better performance in the presence of unknown dynamics.

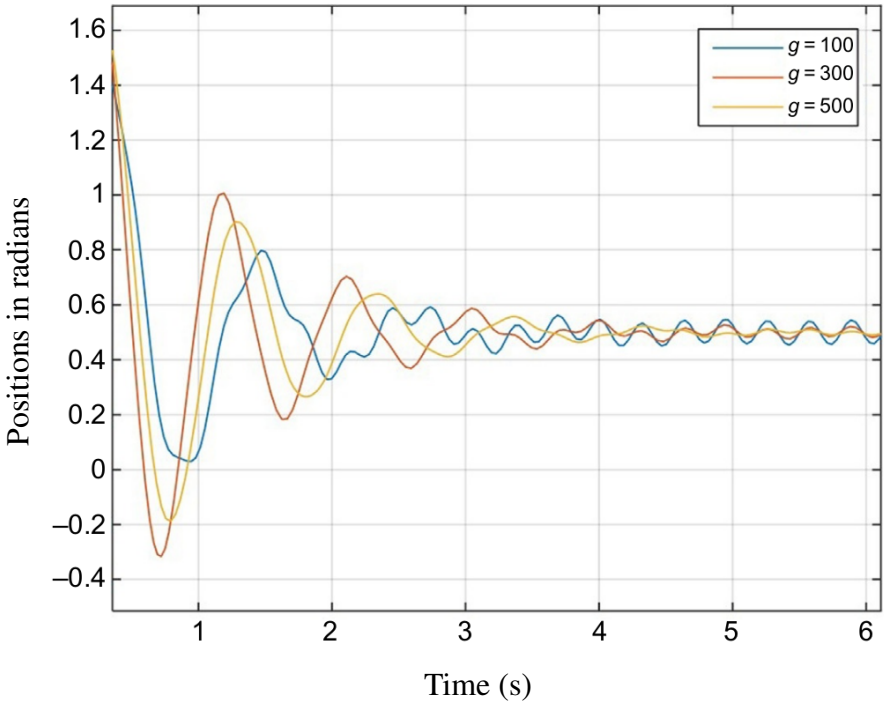

Fig. 4.7: Positional response accompanied by variations in the cut-off frequency of the disturbance observer

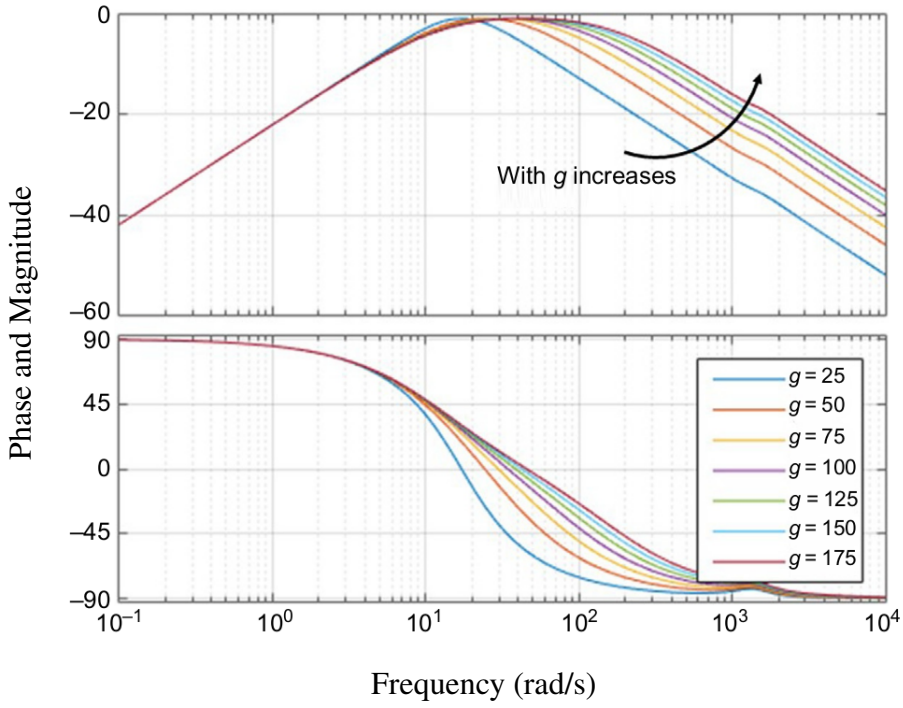

Fig. 4.8: BODE diagram with a cutoff frequency between the RTOB output and disturbance input

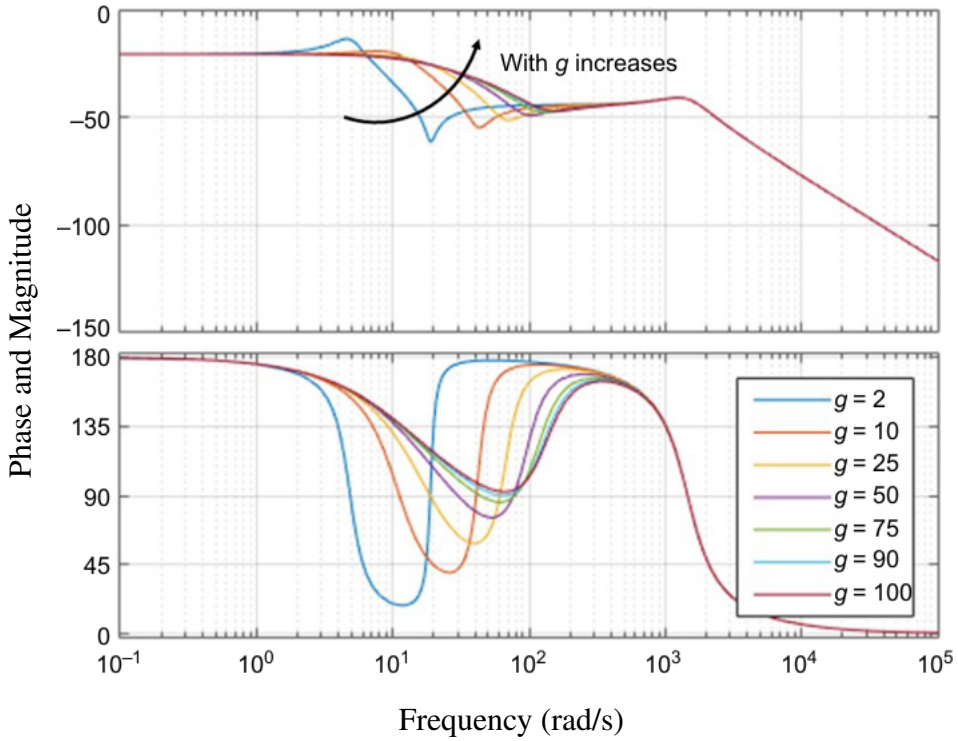

Fig. 4.9: BODE diagram with a cutoff frequency between the positional response and disturbance input

Because the RTOB's LPF filter has a lower cutoff frequency, the outer loop can accurately estimate the reaction force despite external disturbances. A higher cutoff frequency of the DoB's LPF allows for vibration estimation over a wide frequency range. As a result, vibrations with a broad bandwidth can be attenuated. However, the bandwidth is limited by the data acquisition sampling time. For better vibration suppression, a shorter sampling time is always preferred.

According to Equations 4.4, 4.7, and 4.9, the stiffness of the environment in contact affects the setup's ability to control vibration. The behavior of three controller models in relation to the stiffness of the environment is depicted by BODE diagrams in Figure 4.11.

In stiff environments, all three models exhibit consistent behavior. The vibration attenuation in the RTOB-DoB-based model is slightly improved. Therefore, if the environment is stiff, better vibration control can be accomplished. If the contact stiffness with the environment is high, the actuator has a tendency to bounce when there are vibrations. This is evident in the root locus in Figure 4.12.

The system becomes underdamped as the stiffness of the environment increases. Therefore, in addition to the torque vibrations, undesirable vibrations will also be produced at the end effector. This demonstrates how the contact environment affects the force controller's ability to suppress vibration.

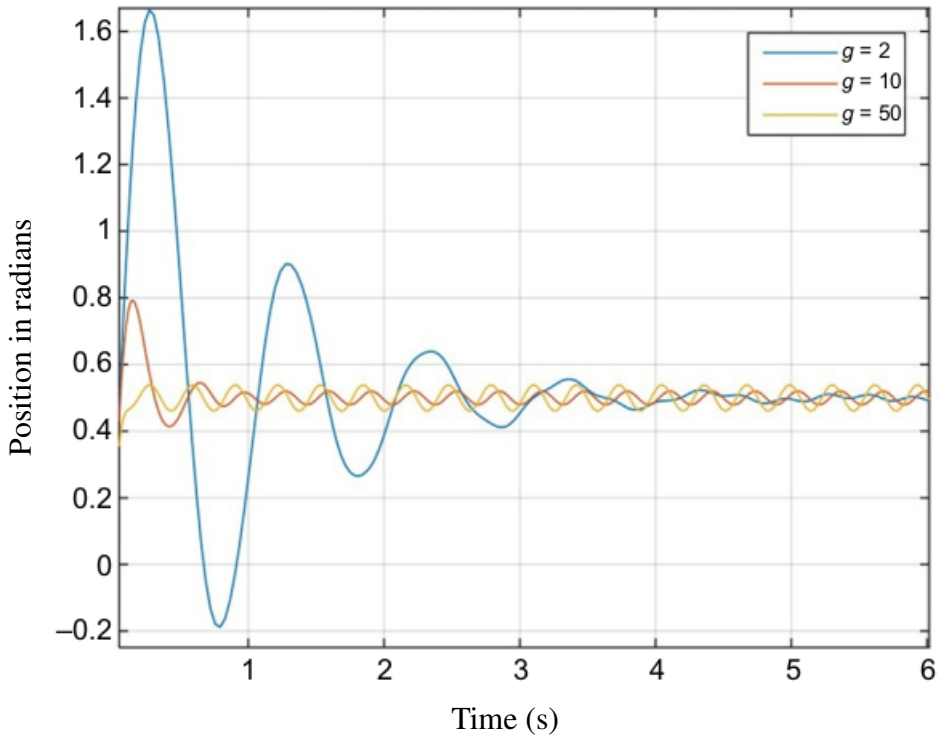

Fig. 4.10: Positional response with variable cutoff frequencies for the reaction torque observer

The simulations make it abundantly clear that conventional force controllers cannot effectively compensate for unknown dynamics. Force controller built on RTOB-DoB is able to account for the dynamics that are unknown. As a result, RTOB-DoB-based force controllers can produce better performances than traditional force controllers.

4.6 Hardware Implementation

Figure 4.13 provides an illustration of the suggested experimental setup that was employed in this chapter. It is made up of a coaxial motor to produce the torque vibrations and a DC motor to drive the force actuator. To demonstrate the contact environment, an object is placed in contact with the actuator arm. In Figure 4.14, the actual test setup is displayed.

Here, the hardware setup is divided into a master and a slave to more easily distinguish between the vibration generator side and the vibration suppression controller side, respectively.

The algorithm has been installed on the microcontroller mbed NXP LPC 1768 [27]. Positions are measured using a 2500 ppr incremental encoder, and current is measured using a current sensor module with differential amplifiers. For data storage, an SD card reader is connected using the SPI protocol. The following subsections contain more

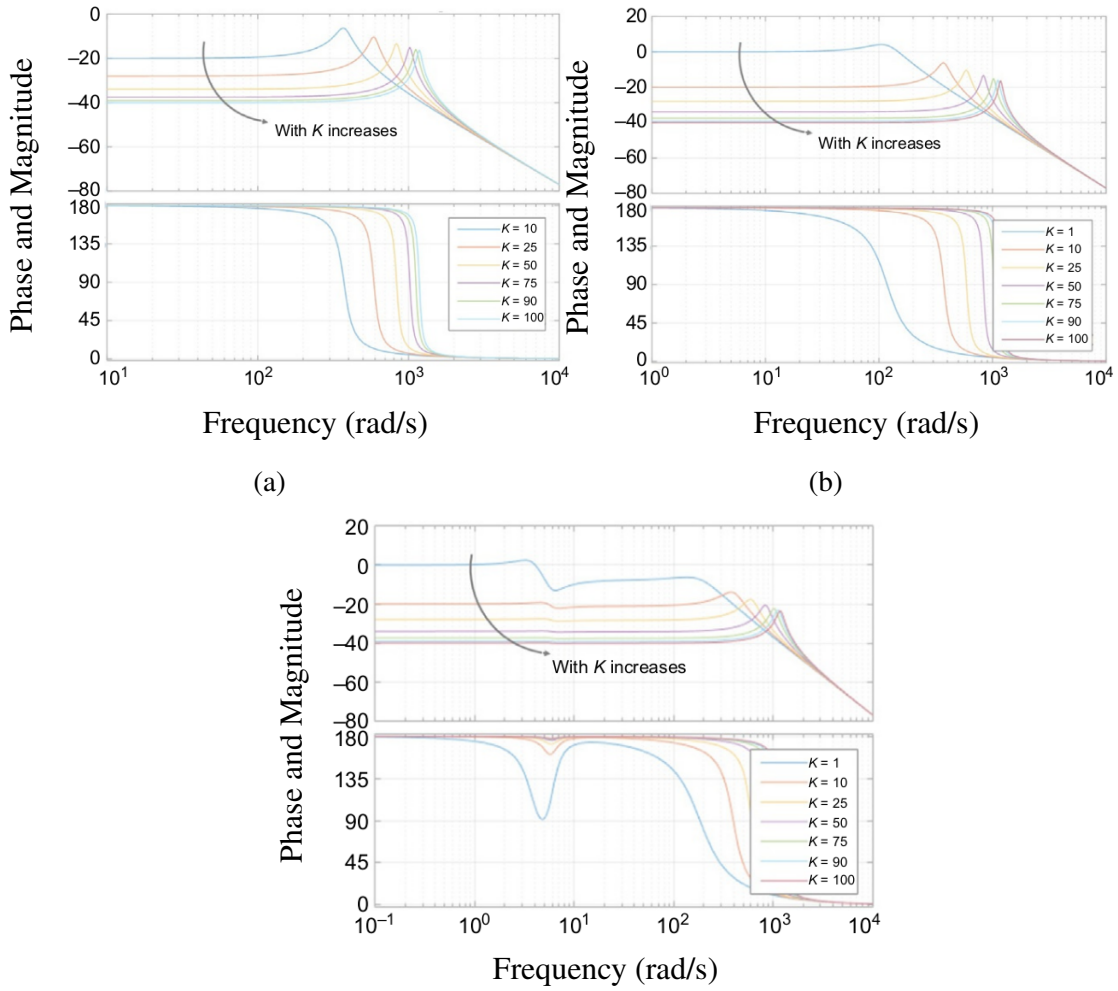

Fig. 4.11: The BODE diagrams illustrating the effects of changes in the environment's stiffness on disturbance input and positional response are available for three force controller models: (A) the current controlled model, (B) the reaction torque observer-based (RTOB) model, and (C) the RTOB and disturbance observer-based model.

in-depth information on the components.

4.7 Subsystems in the hardware configuration

The hardware setup that has been implemented essentially consists of 5 different sub-modules. These will be discussed in this section in brief.

1. Power unit.

2. mbed microcontroller and SD card reader-based module.

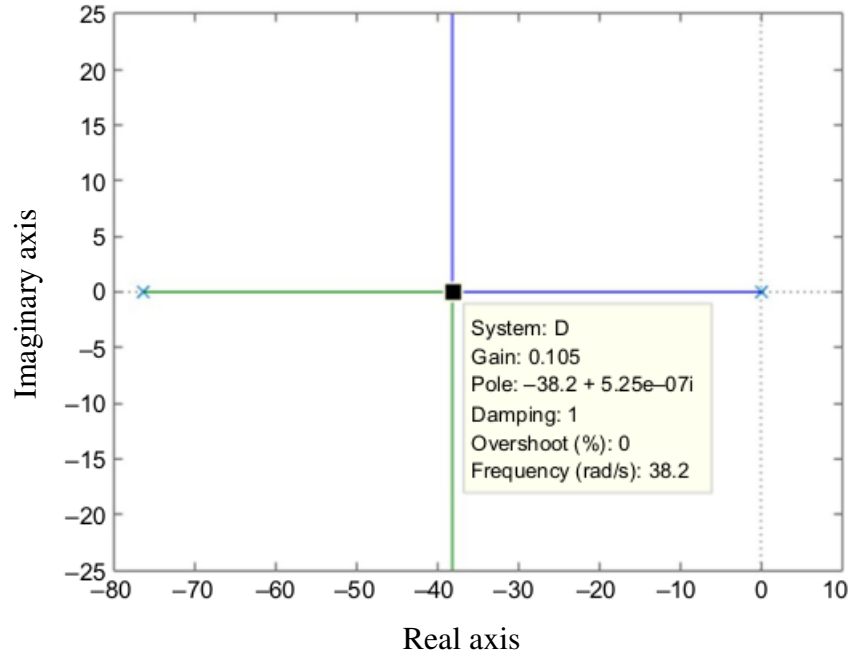

(a)

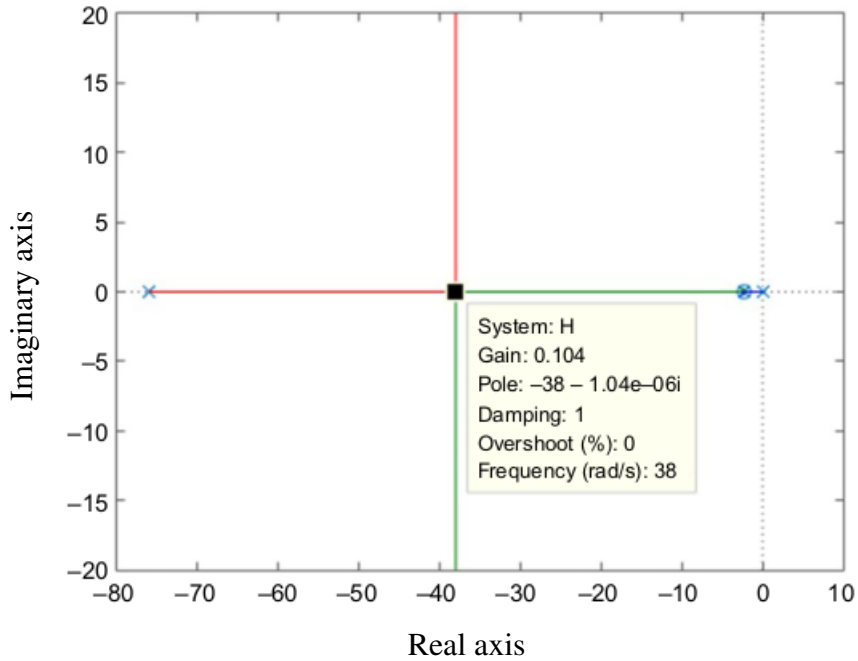

(b)

Fig. 4.12: The root locus of two force control models (A) the current-controlled model and (B) the reaction torque observer-based model - are analyzed with respect to changes in the stiffness of contact environments

3. Auxiliary mbed microcontroller-based module.

4. Current sensor module.

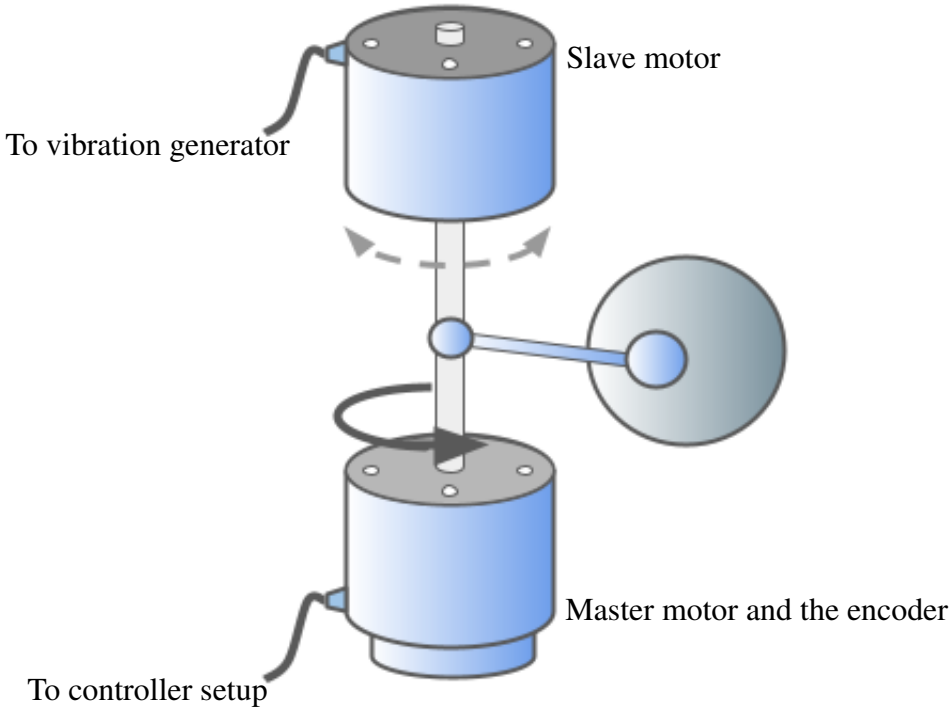

Fig. 4.13: Sketch representation of the experimental setup

5. DC motor driver.

The five different modules are designed to make it simple to produce, manage, analyze, and troubleshoot these units. Figure 4.15 displays the hardware-based functional block diagram for the master side.

4.7.1 Power unit

Two transformers are used to supply the entire unit's power needs. The primary side input of the transformers is 230 VAC, and the secondary outputs are rectified and smoothed to produce the desired regulated DC power supply. The DC motors are powered by one transformer, and the auxiliary circuits are powered by the other.

The power flow diagram, which is depicted in Figure 4.16, details how the power is allocated among the modules.

4.7.2 mbed microcontroller and SD card reader-based module

The mbed microcontroller is centralized in this module. This has four input interfaces: two for master and slave side current sensors, one for the master side encoder, and one for the SD card. A 15V DC supply has been injected, which powers the mbed

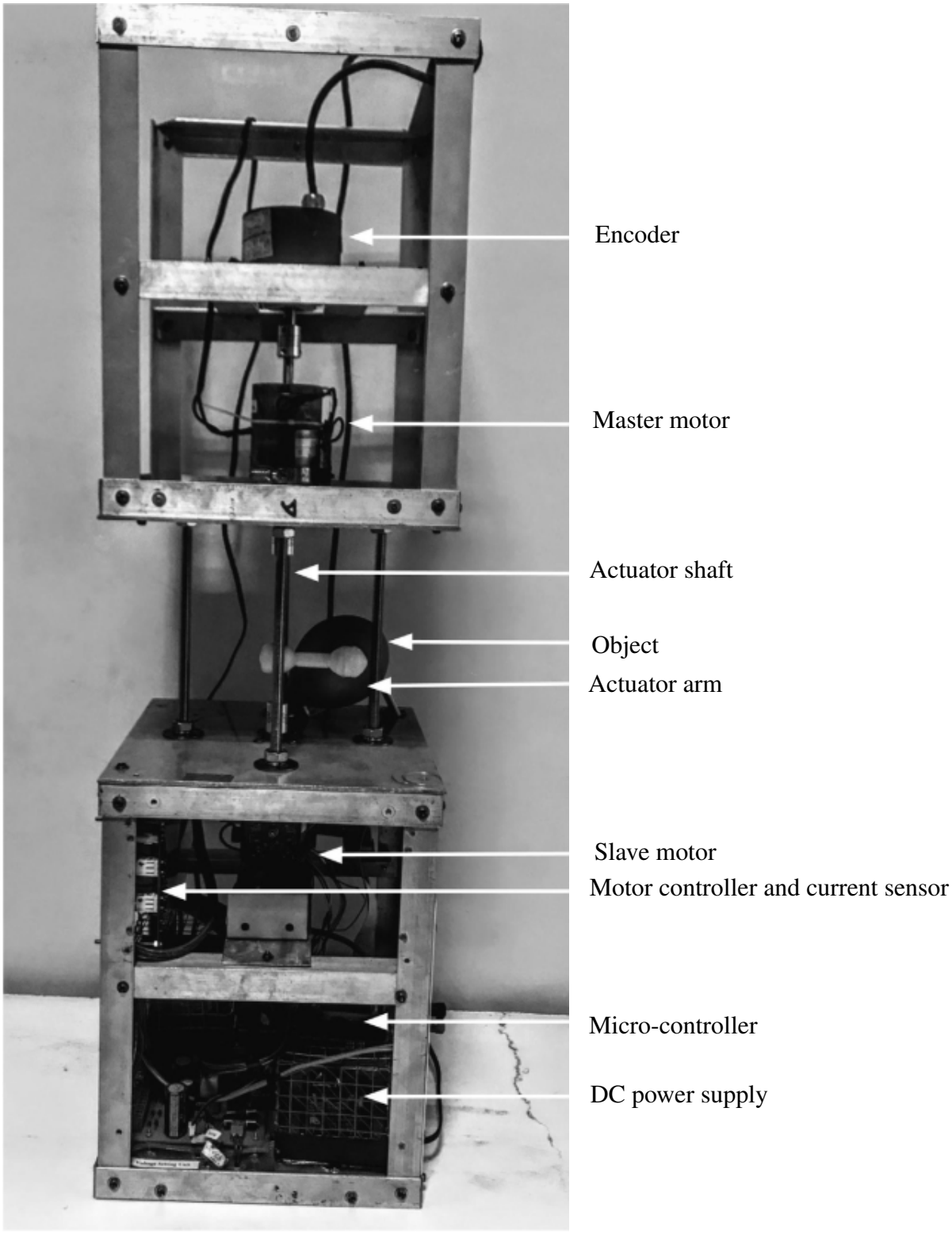

Fig. 4.14: Experimental setup

microcontroller, two encoders, and the SD card module. The motor driver module and the main microcontroller are connected via an output interface link, which is used to

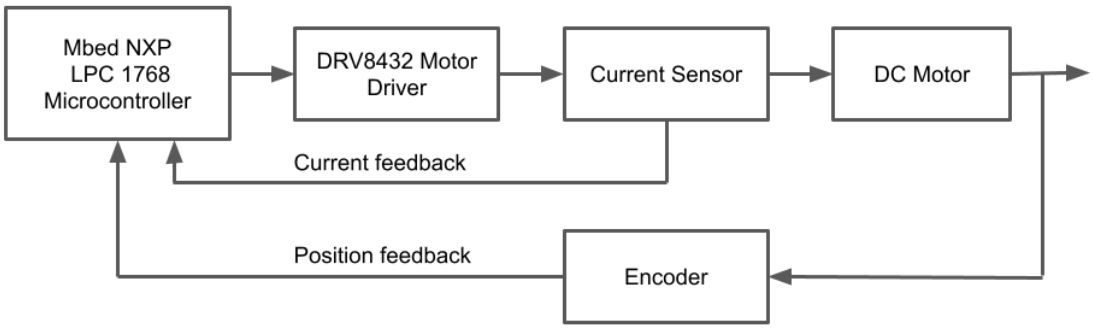

Fig. 4.15: Master side functional block diagram

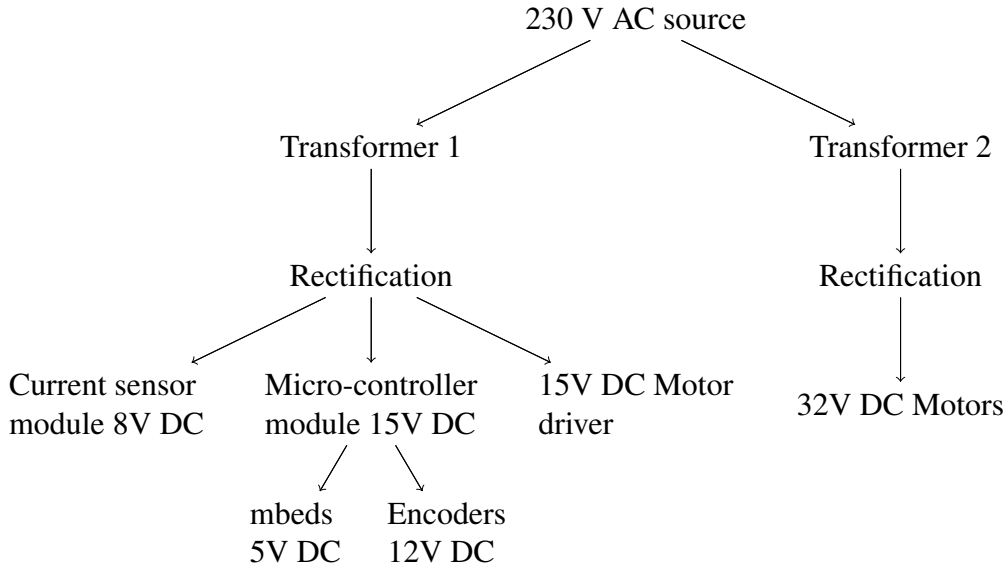

Fig. 4.16: Power flow diagram in the experimental setup

transmit commands. The encoder interface on the master side motor provides position feedback, whereas the current sensor interfaces are connected to current sensors on both motors.

The data is stored on an SD card reader module for later analysis and results recording. Since the data recording process requires a lot of time, it was processed in a parallel thread to cut down on the algorithm's cycle time. A high cycle time can lower the algorithm's accuracy, which has a negative impact on system performance. A serial peripheral interface (SPI) connection was used to connect this SD card module to the mbed microcontroller.

4.7.3 Auxiliary mbed microcontroller-based module

The experiment setup makes use of two mbed microcontrollers. The master motor encoder readings are transmitted to the primary mbed microcontroller via the auxiliary mbed microcontroller module. Using a 100Mbps half-duplex ethernet link, data was

transferred between two mbed modules. The structural arrangement of the auxiliary mbed-based module is the same as that of the main mbed-based module, with the exception that it does not include the SD card reader interface.

4.7.4 Current sensor module

This setup uses internal DoB and RTOB sensing mechanisms for external force estimation, and one of the two controller inputs is current feedback from the motors. Accurate current sensing of the motors is therefore crucial. Consequently, it is imperative to have a current sensor that is extremely sensitive and can even detect changes in current at the milliampere level.

The two components of this current sensor module are a current transducer and a differential amplifier, which amplify the transducer signal before it is fed to the microcontroller. Essentially, each of the current sensors is sending out a single output, which is later transformed into a vector with a direction and a value component. The provided image in figure x, which elaborates on the current measurement process, clarifies this further.

This module uses two ACS712t 5A type current transducers that can measure the instantaneous current flowing through a conductor. As shown in Figure 4.17, these transducers produce a voltage between 1.7 and 3.3 volts that is later converted to a vector by using 2.5 volts as the zero reference. In this case, 3.3V stands for 5 A and 1.7V DC for the -5A limit. Using differential amplifiers, these signals, which are between 2.5V and 3.3V DC, are then stepped up to a voltage between 0V DC and 3.3V DC. Additionally, using differential amplifiers, the voltages between 1.7 and 2.5 volts were changed to map in the DC range of -3.3 to 0 volts.

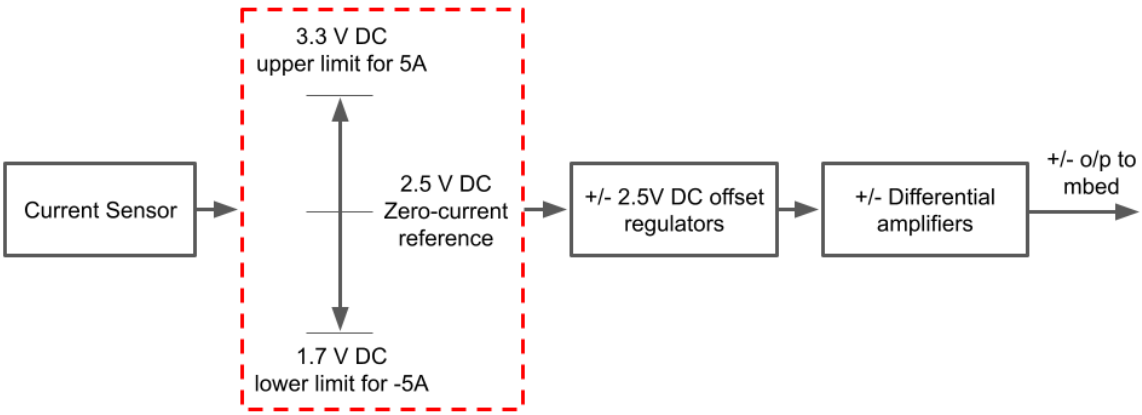

Fig. 4.17: The procedure for the current measure

4.7.5 DC motor driver

The motor control board that was built for this experiment is depicted in Figure 4.18. The chosen driver IC is the DRV 8432 dual full bridge PWM motor driver. For high-current applications, it is not advised to use one DRV 8432 driver for two DC motors, though it is technically possible. As a result, the motor control board has two drivers installed for the two DC motors used by the slave and master actuators.

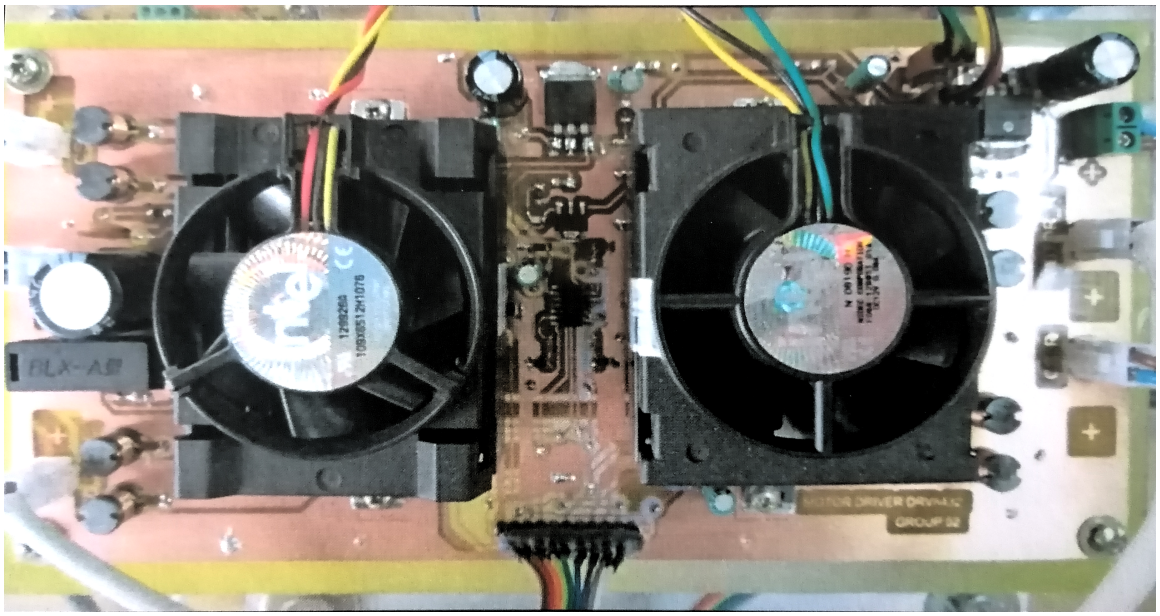

Fig. 4.18: Motor control board based on DRV 8432 drivers

In addition to offering high performance, the DRV 8432 also has a strong protection system that guards the system against various fault scenarios. This driver package includes a substantial heat sink on top of the driver to effectively dissipate heat. Two 12V supplies are injected into this module, one for the DRV 8432 drivers and the other for the H bridges.

The motor can run at a low current change rate under typical operating conditions because of its adequate inductance. However, due to high current fluctuation rates and low system impedance, it is possible for the motor to draw a high enough current to exceed the maximum current when it is in a short circuit condition. External inductors have been used to combat this, preventing the system's current from fluctuating suddenly. The fact that DRV 8432 offers extremely high efficiency at relatively high switching frequencies, like 500 kHz, is one of the main arguments for choosing it. Additionally, a wide range of input and output duty cycle values can be operated at high frequencies.

4.7.6 Control board

The mbed LPC-1768, a 96 Mhz microcontroller, is used to operate the DC motors. A well-liked online tool for quickly and securely prototyping microcontroller-based systems is called mbed. It is a low-cost, low-power gadget. With 512 KB of brand-new memory and 64 KB of SRAM, it has a potent 32-bit Arm Cortex M3 processor operating at 96 MHz. On the mbed board, which has a 40 pin DIP connector with a 0.1 inch pitch, LPC-1768 is mounted. C++ can be used to write programs, which can then be compiled and downloaded for use on the mbed NXP LPC-1768 microcontroller. Furthermore, nothing needs to be installed; almost everything, including the compiler, is available online.

4.7.7 DC motors

For both the master and slave units, two identical DC motors from the same manufacturer have been used. The motors are permanent magnetic DC motors of the brushed type. An encoder that is coupled to the master motor is used to measure position, velocity, and acceleration.

4.7.8 Encoder

An incremental rotary encoder is used to track the position of the end effector. In order to improve resolution, a quadrature encoder interface is applied to this encoder.

To achieve the high accuracy needed, an optical incremental rotary-type encoder with 5,000 pulses per revolution has been used in conjunction with the master motor. The appendix 2 contains the master encoder's specification. This resolution has been raised to 20,000 pulses per revolution using techniques for quadrature encoder interfaces.

4.8 Experimental setup configuration and results

The pre-estimated system parameters and configurational values for the experiment are listed in Table 4.2. The slave coaxial motor in the practical experiment produced a 20 Hz vibration torque with a 0.027 Nm amplitude, as shown in Figure 4.19. After that, a 0.135 Nm torque was applied to the force-actuating motor in order to record the positional response of the current control-based force controller. The positional response of the current control-based force controller is shown in Figure 4.20. The standard deviation of the positional response was 61.4 rad.

By adjusting the cutoff frequency of the DoB's low pass filter, positional responses of a reaction torque observer plus disturbance observer-based force controller were obtained for the same disturbance torque and torque command. The position response at

TABLE 4.2: SYSTEM SETTINGS AND PARAMETERS USED IN THE EXPERIMENT

Parameter	Description	Value
K_{tn}	Nominal motor torque constant	0.135 Nm/A
J_n	Nominal motor inertia	0.000072 kgm^2
τ_{ref}	Torque reference	0.15 Nm
K_p	Controller proportional gain constant	12000
K_d	Controller derivative gain constant	0
K_i	Controller integral gain constant	0
g_{dis}	DoB LPF's Cut-off frequency	100 rad/s
g_{RTOB}	RTOB's LPF's Cut-off frequency	5 rad/s
B	DC motor viscous friction coefficient	0.000001 Nms/rad
τ_f	Static friction constant	0.025 Nm
dt	Sampling time	200 μs

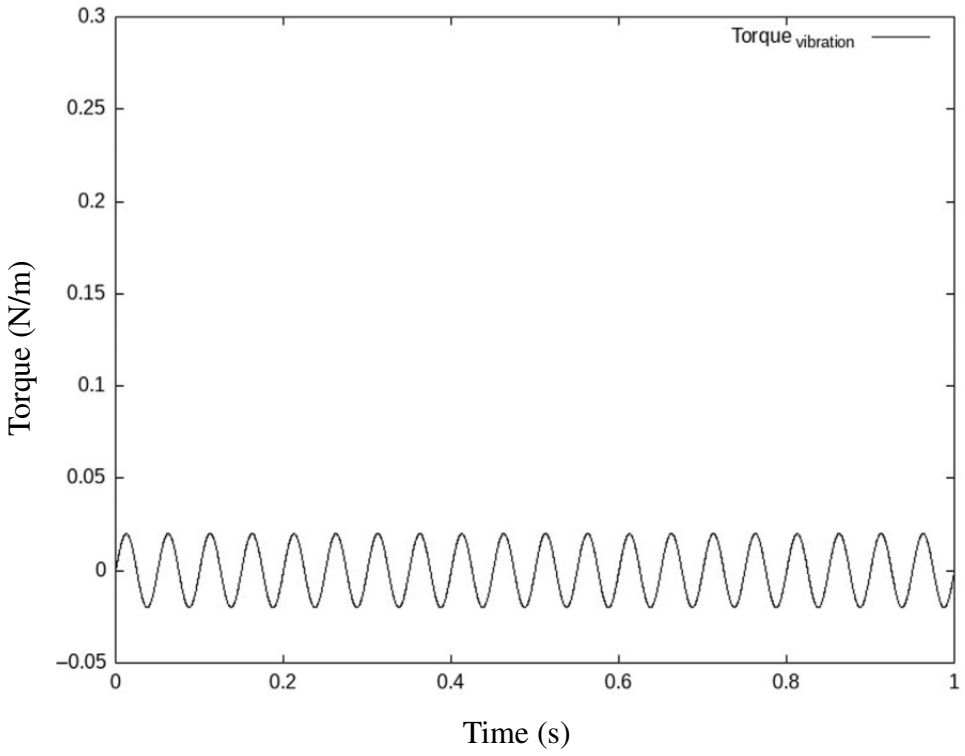

Fig. 4.19: Sinusoidal shaped torque vibration

300 rad/s g_{dis} is shown in Figure 4.21. This positional response had a 52.454 rad standard deviation. Figure 4.22 and Figure 4.23, which represent the positional responses for g_{dis} 250 and 150, respectively. Their respective standard deviations were 53.4652 and 53.9754 rad.

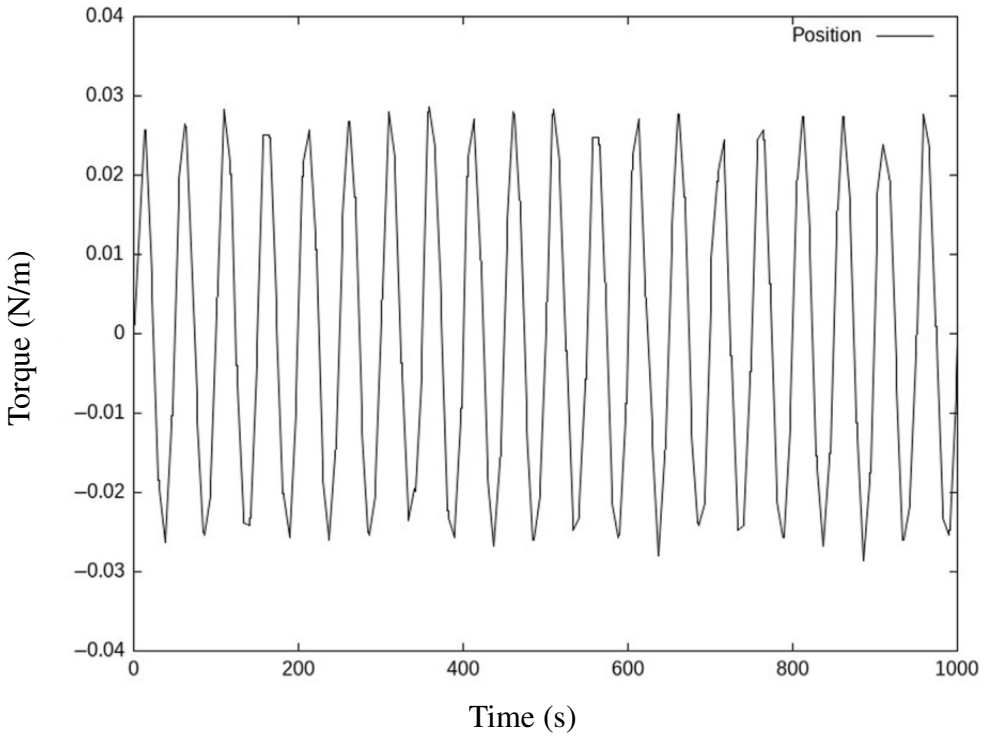

Fig. 4.20: The positional response of a force controller based on current control.

The standard deviation values obtained from the experiment are summarized in Table 4.3. These demonstrate that high cutoff frequencies (g_{dis}) improve vibration suppression performances. However, due to hardware restrictions, experimental results are restricted to a g_{dis} value of 300 rad/s.

TABLE 4.3: THE STANDARD DEVIATION OF POSITIONAL RESPONSES WAS CALCULATED FOR EACH EXPERIMENT

Experiment	Standard deviation (rad)
Force controller with RTOB-DoB when g_{dis} is 300 rad/s	52.454
Force controller with RTOB-DoB when g_{dis} is 250 rad/s	53.4652
Force controller with RTOB-DoB when g_{dis} is 150 rad/s	53.9754
Current-based force controller	61.4

4.9 Conclusion

By using disturbance observers, force controller vibrations can be reduced. External coaxial vibration torques cause positional and forced vibrations in the force actuators' force-exerting ends. These vibrations are transmitted to the environment that the forces

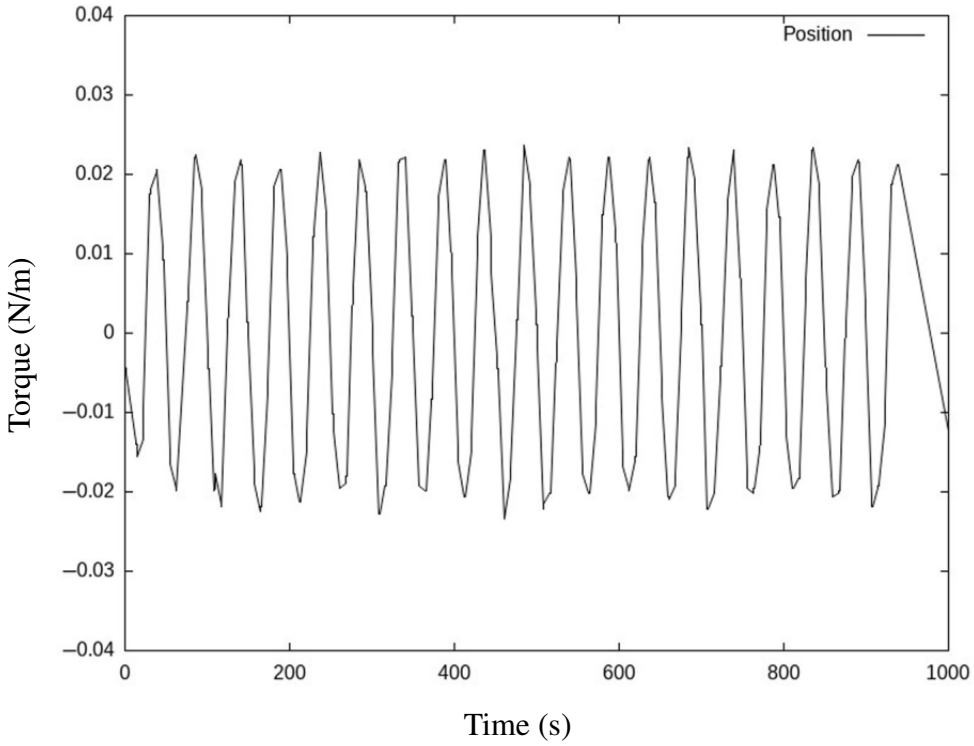

Fig. 4.21: When $g_{dis} = 300 rad/s$, the positional response of the force controller that uses both reaction torque observer and disturbance observer (RTOB-DoB)

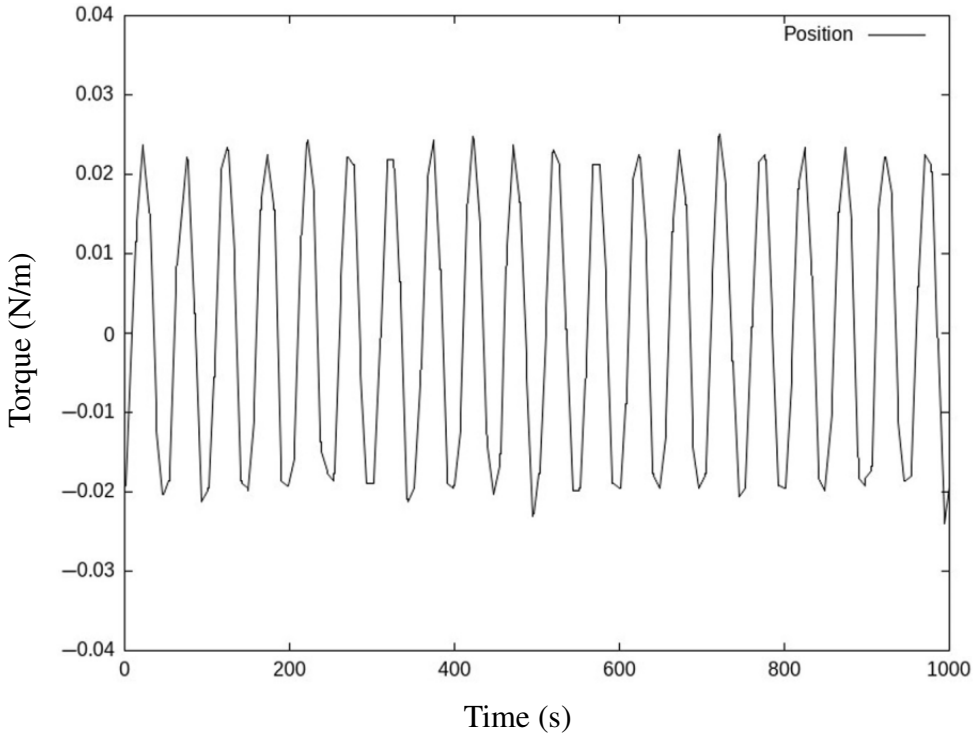

Fig. 4.22: When $g_{dis} = 250 rad/s$, the positional response of the force controller that uses both reaction torque observer and disturbance observer (RTOB-DoB)

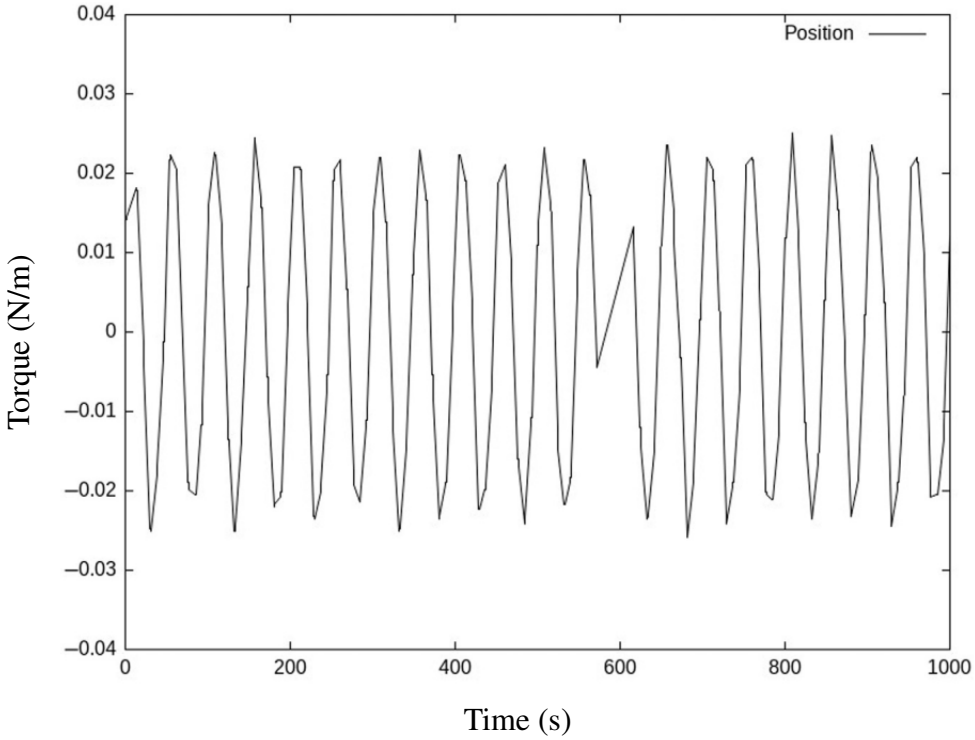

Fig. 4.23: When $g_{dis} = 150rad/s$, the positional response of the force controller that uses both reaction torque observer and disturbance observer (RTOB-DoB)

are in contact with. This, in turn, degrades the performance of force controllers. By maintaining a constant reaction force between the object and the force actuator, these vibrations can be reduced. However, conventional force control techniques that rely on present controllers and force sensors are unable to accomplish this. This chapter introduced a force sensorless force-control technique that could dampen vibrations. There, disturbances were calculated and fed back by the inner loop DoB to account for the disturbances. The reaction force was estimated and provided feedback on using an outer loop RToB, a DoB variant. DoB's LPF cutoff frequency was increased to better capture the vibrations. In contrast, a lower value was set for the RTOB's LPF cutoff frequency in order to calculate the steady reaction force.

The proposed force control method and conventional force control methods were compared using simulations for the purpose of vibration suppression. The proposed method performed better than the traditional methods, according to analytical findings that were based on the simulations. Additionally, simulation results demonstrated that by appropriately raising the DoB LPF's cutoff frequency, vibration suppression could be improved. The cutoff frequency of the DoB was, however, constrained to a maximum by the microcontroller's sampling time. An actual experiment was carried out to confirm the simulation results. This leads to the conclusion that using disturbance observers can reduce force controller vibrations.

CHAPTER 5

STUDY OF STABILITY VARIATIONS IN REACTION TORQUE OBSERVER-BASED FORCE CONTROLLERS

5.1 Introduction

System modeling is a crucial aspect of designing a motion control system. However, the limitations of modeling techniques lead to modeling uncertainties. These modeling uncertainties lead to unpredictable and unstable control systems [25], [28]. For instance, a spring and damper are frequently used to represent the environment in contact [29], [14]. Traditionally, when tuning the force controller, the spring and damper are thought to have constant coefficients throughout the motion. However, the research work in [14] has shown that the properties of the environment in contact exhibit a dynamic and nonlinear nature when motion parameters are altered. Consequently, in some applications, the traditional approach to control system design is vulnerable. Utilizing a reaction torque observer (RTOB), which is a variation of the disturbance observer (DoB) concept, is a successful way to ascertain the unpredictable environmental impedance. By combining RTOB and DoB, a force controller that is both robust and accurate can be created.

Fulfilling the safety and functionality requirements for motion systems is a challenging but essential task. Therefore, it is essential to design controllers with stable behavior while maintaining robustness. This study investigates the potential instability of RTOB-based force controllers. The two cut-off frequencies for DoB and RTOB are typically assumed to always be equal to one another when examining a RTOB-based force controller. But occasionally, it cannot keep the stability. The stability of the system is determined by the interactions between the mechanical, environmental, and controller dynamics, which also add to the design constraints. There has not been any analysis of unstable scenarios in terms of system dynamics.

This chapter investigates the potentially unstable scenarios of RTOB-based motion systems in the presence of unpredictability in the environment in contact. It also suggests a method for choosing the controller parameters that are unique to an application in order to achieve greater stability. The importance of system inertia to the stability of the system is covered in the final section. The simulation results are used to confirm the validity of the proposals.

5.2 Modelling

The force controller that is integrated with DoB and RTOB is shown in Figure 5.1. The controller gain is represented by K_p. To translate to the current domain, the nominal

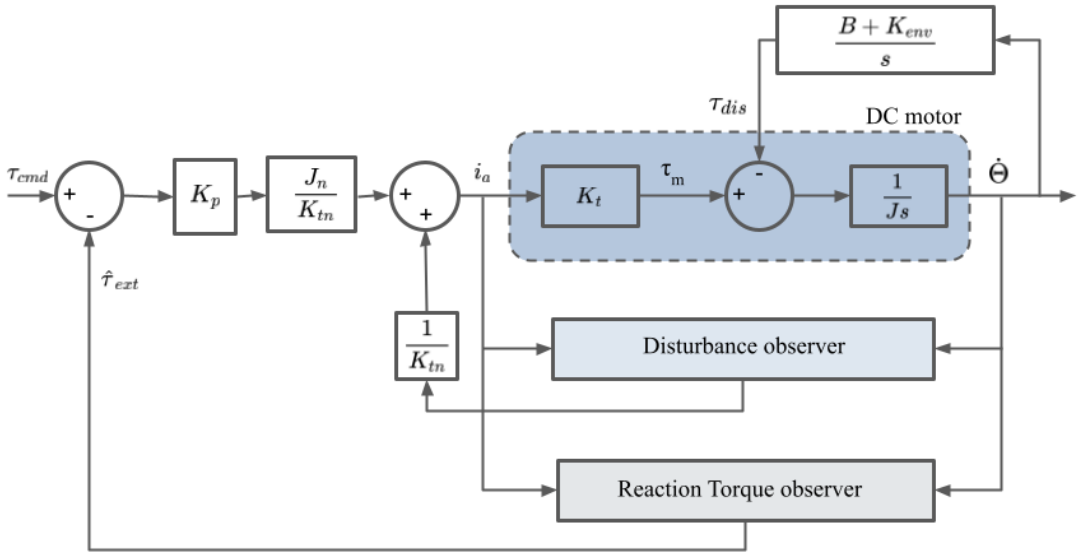

Fig. 5.1: Force control system with the environment modeled as a spring and damper

inertia/nominal torque constant factor is multiplied by the amplified force error. The output of the disturbance observer is fed back into the system after being divided by the nominal torque constant in the inner loop to increase the robustness of the controller. The environment in which the disturbance torque is applied is simulated using a spring damper.

The transfer function between the force command and the reaction torque observer estimation is represented by Equation 5.1, which is derived from Figure 5.1.

$$\frac{\hat{\tau}_{ext}}{\tau_{cmd}} = \frac{as^2 + bs + c}{As^4 + Bs^3 + Cs^2 + Ds + E} \tag{5.1}$$

where,

a $Bg_{RTOB}JK_p$
b $g_{RTOB}JK_p(Bg_{dis} + K_{env})$
c $g_{dis}g_{RTOB}JK_{env}K_p$
A J
B $B + g_{dis}J + g_{RTOB}J$
C $Bg_{RTOB} + g_{dis}g_{RTOB}J + K_{env} + Bg_{RTOB}JK_p$
D $g_{RTOB}K_{env} + Bg_{dis}g_{RTOB}JK_p + g_{RTOB}JK_{env}K_p$
E $g_{dis}g_{RTOB}JK_{env}K_p$

5.3 Study of Stability

Stability is studied using equation 5.2, which is the characteristic equation derived from equation 5.1.

$$As^4 + Bs^3 + Cs^2 + Ds + E = 0 \tag{5.2}$$

The Routh Hurwitz criteria is then applied to the resultant characteristic equation, and conditions are derived as in equation 5.3.

$$f_1 = \frac{\begin{array}{c}(B + g_{dis}J)(Bg_{RTOB} + g_{RTOB}(g_{dis} + g_{RTOB})J + K_{env}) \\ +g_{RTOB}J(B^2 + Bg_{RTOB}J - JK_{env})K_p\end{array}}{B + g_{dis}J + g_{RTOB}J} > 0 \tag{5.3}$$

Stability can be described as a function of six variables in relation to the equation above. Environmental factors, mechanical variables, and controller variables are the three categories into which they can be separated. Motor inertia J is classified as a mechanical variable, while the controller gain K_p , the cut off frequencies of the DoB (g_{dis}) and the $RTOB$ (g_{RTOB}), can be listed under controller variables. K_{env} and B_{env} can be categorized for the environmental variables because the environment in contact is modeled as a spring damper.

Environmental variables are considered unpredictable since they often change in response to dynamic situations like temperature and environmental contraction, among other things. The study assumed four alternative settings as soft, neither soft nor hard, hard, and hardest to remove these environmental factors from the equation.

5.4 Simulations

TABLE 5.1: ENVIRONMENT CONSTANT VALUES USED IN SIMULATIONS

Environment Nature	K_{env}	B_{env}
Soft	10 Nm/rad	0.01 Nms/rad
Neither hard or soft	100 Nm/rad	0.01 Nms/rad
Hard environment	1000 Nm/rad	0.01 Nms/rad
Hardest environment	1000 Nm/rad	0.1 Nms/rad

The stability conditions that were determined were made visible in three dimensions by modifying the mechanical and controller settings. Figure 5.2 depicts the simulations for the soft environment as graphs. Going from left to right, the illustration shows the impact of controller gain variation. The second row of the graphic is obtained by assuming that the system has a higher inertia. The identical simulations for the three additional environmental models are depicted in Figures 5.3, 5.4, and 5.5. The horizontal axes in a particular graph reflect the g_{RTOB} and g_{dis} values. On the

vertical axis, the value of the function f_1 is shown. Two different color schemes were used to distinguish between stable and unstable zones. Yellow zones represent the potential dynamic parameter combinations that could stabilize the system. The blue area is used to display the unstable combinations. The environmental constants utilized in the simulation are listed in Table 5.1.

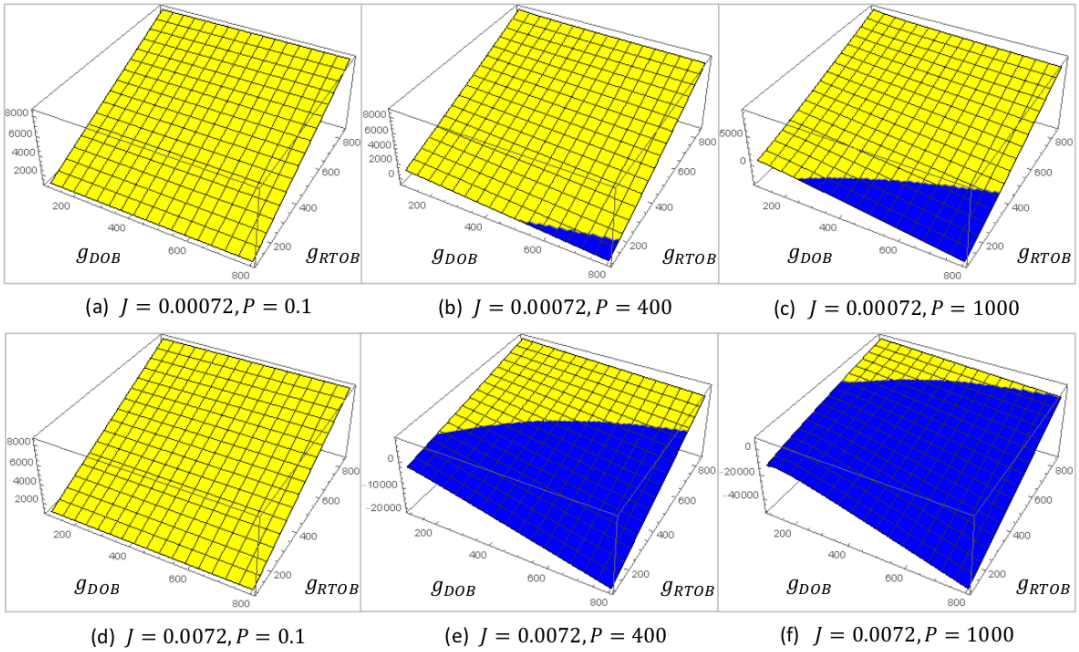

(a) $J = 0.00072, P = 0.1$ (b) $J = 0.00072, P = 400$ (c) $J = 0.00072, P = 1000$

(d) $J = 0.0072, P = 0.1$ (e) $J = 0.0072, P = 400$ (f) $J = 0.0072, P = 1000$

Fig. 5.2: Observation of Stability Variation under Soft Environment

Figures 5.6, 5.7, and 5.8 depicts the time domain study that was performed to validate the stability analysis. Figure 5.6 is created by altering the controller gain. Table 5.2 lists the mechanical and controller parameters for the time domain study. Figure 5.7 shows the instability that results when the inertia varies but the other factors don't. Figure 5.8 illustrates how the stiffness of the environment affects stability. Figure 5.9 shows an instance where a system is stabilized by changing the cutoff frequency values independently while keeping the other parameters fixed.

The stability zones get smaller as the controller gain increases, as shown in figures 5.2, 5.3, and 5.4. The controller gain effect is confirmed by the time domain response as depicted in Figure 5.6. It has been demonstrated that the experiments performed at higher inertial values are highly unstable. This issue has been addressed by suggesting the use of lower controller gains. Force tracking performance, however, will be poor. In accordance with the analysis shown in Figures 5.3, 5.4 and 5.5, the stability is also attained by independently adjusting the cutoff frequencies while maintaining the other parameters at the desired values.

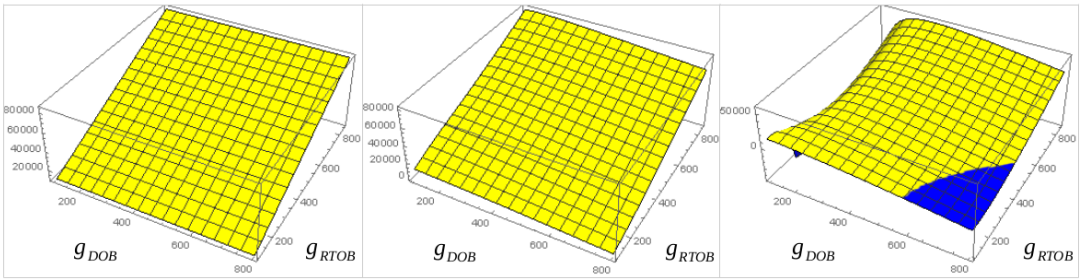

(a) $J=0.00072, P=0.1$ (b) $J=0.00072, P=400$ (c) $J=0.00072, P=1000$

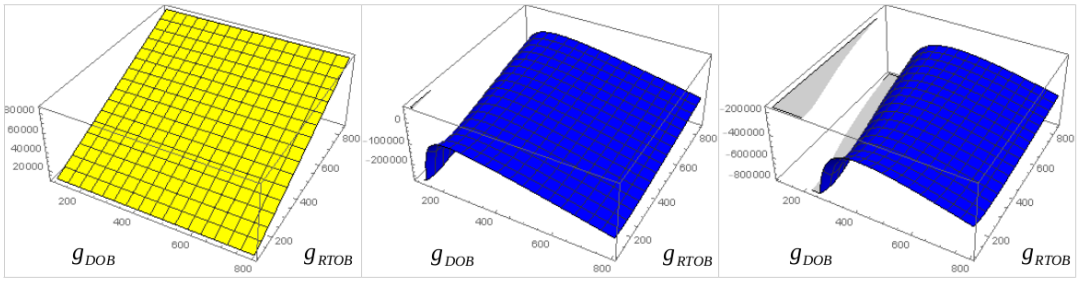

(d) $J=0.0072, P=0.1$ (e) $J=0.0072, P=400$ (f) $J=0.0072, P=1000$

Fig. 5.3: Observation of Stability Variation under neither hard or Soft Environment conditions

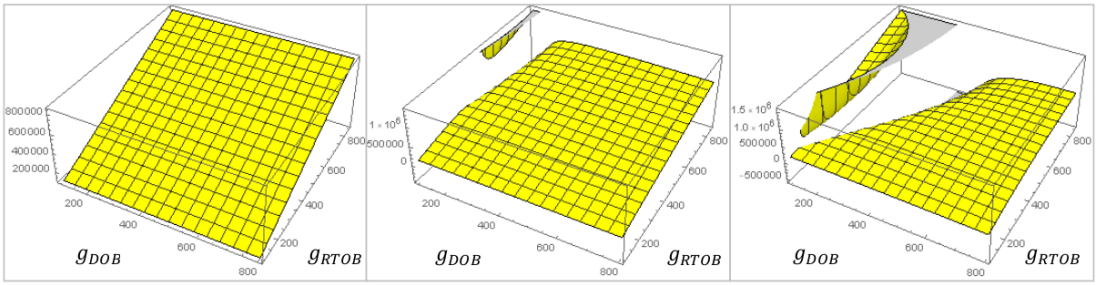

(a) $J = 0.00072, P = 0.1$ (b) $J = 0.00072, P = 400$ (c) $J = 0.00072, P = 1000$

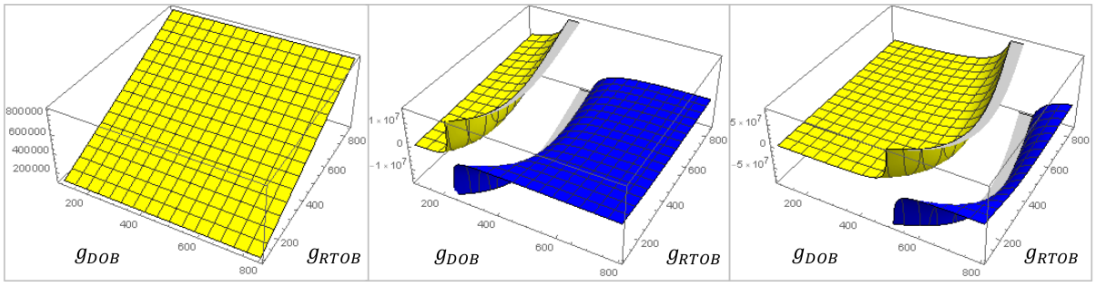

(d) $J = 0.0072, P = 0.1$ (e) $J = 0.0072, P = 400$ (f) $J = 0.0072, P = 1000$

Fig. 5.4: Observation of Stability Variation under hard Environmental conditions

5.4.1 Conclusion

This research explores the factors that contribute to the instability of force controllers utilizing $RTOB$, highlighting the importance of mechanical, environmental, and controller dynamics for stability. To assess stability for such systems, a novel approach is

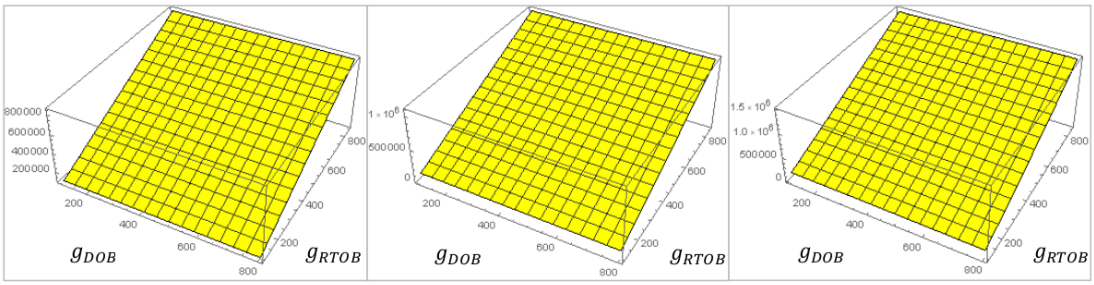

(a) $J = 0.00072, P = 0.1$ (b) $J = 0.00072, P = 400$ (c) $J = 0.00072, P = 1000$

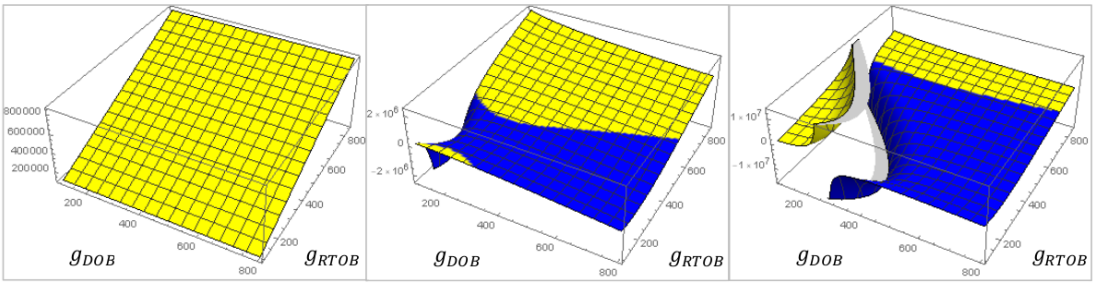

(d) $J = 0.0072, P = 0.1$ (e) $J = 0.0072, P = 400$ (f) $J = 0.0072, P = 1000$

Fig. 5.5: Controller gain is varied

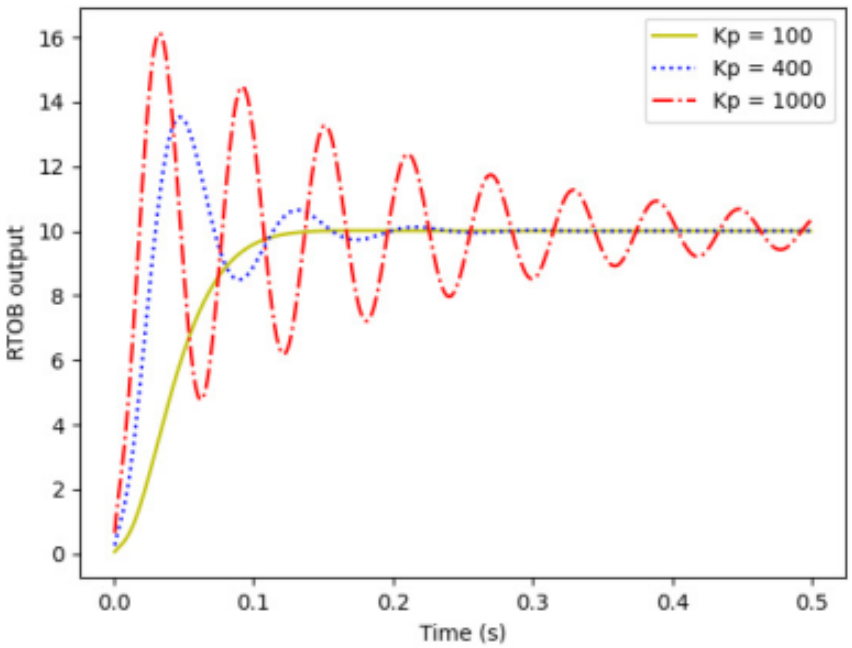

Fig. 5.6: Time domain response with controller gain variation

introduced, which considers the contact environment as a spring damper and derives a transfer function to apply the Routh Hurwitz stability criterion. Through analyzing various mechanical, environmental, and controller parameters, this study provides a concise yet precise stability condition.

The mechanical parameter, inertia J, is found to be crucial for maintaining stability.

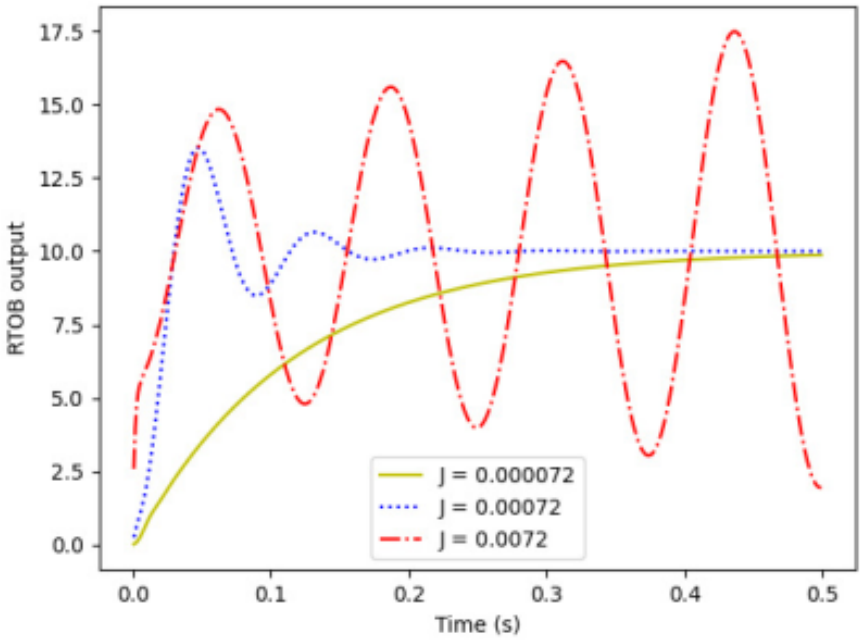

Fig. 5.7: Time domain response when system inertia is varied

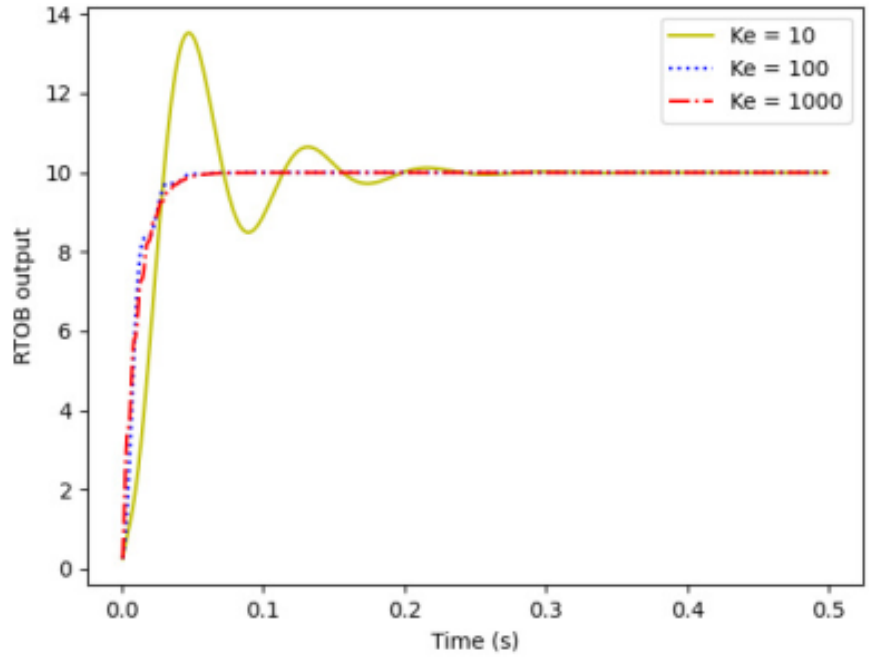

Fig. 5.8: Time domain response when environment stiffness change

Specifically, force controllers based on $RTOB$ may become unstable at higher inertial values, and reducing the controller gain can stabilize the system at the expense of force tracking performance. This study proposes a method to effectively tune the two cutoff frequencies separately, ensuring that g_{dis} is less than g_{RTOB}.

Moreover, stability significantly depends on the environment. In cases where

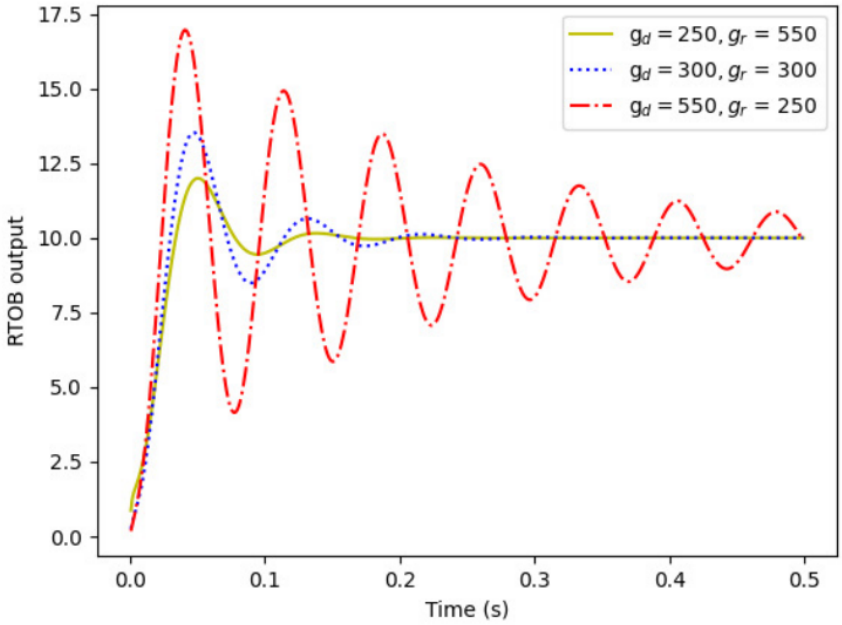

Fig. 5.9: Stabilization of the reaction torque observer through individual adjustments to the cutoff frequencies of the disturbance observer and the reaction torque observer

TABLE 5.2: MECHANICAL AND CONTROLLER PARAMETERS USED WITH THE TIME DOMAIN STUDY

Parameter	Description	Value
J_n/J	Nominal/ Actual Inertia of the motor	0.00072 Nm
K_{tn}/K_t	Nominal/ Actual torque constant	0.135 NmA^{-1}
B	Absolute Viscous friction coefficient	0.01 Nms/rad
B_m	Motor Viscous friction coefficient	0.01 Nms/rad
K_{env}	Stiffness of the environment in contact	10 Nm/rad
g_{DoB}	Cut off frequency value in DoB	300 s^{-1}
g_{RTOB}	Cut off frequency value in RTOB	300 s^{-1}

the contact environment has lower stiffness, the controller should be tuned to satisfy $g_{dis} << g_{RTOB}$. However, if the environment has higher stiffness, it is best to keep $g_{dis} = g_{RTOB}$. Viscosity, a parameter beyond the designer's control, can also impact stability.

The study's findings highlight the importance of carefully selecting the right parameter combinations when designing a force controller utilizing DoB and $RTOB$.

CHAPTER 6

CONCLUSION

In conclusion, Reaction Torque Observer (RTOB)-based controllers have proven to be an effective alternative to traditional force sensors in various motion control systems. These controllers bring multiple benefits, including variable bandwidth, the capability to estimate unknown disturbances, and the ability to feed back disturbances to enhance system robustness.

The model-based architecture of these systems makes parameter estimation a critical component. This thesis investigated stability variations in RTOB-based motion systems and developed recommendations for optimizing controller parameters. The study emphasized that the stability of these systems heavily relies on the accuracy of system parameters. Accordingly, a rapid and precise method for parameter estimation was developed to minimize computational expenses.

High-frequency external vibrations, such as those from infrastructure, can adversely affect system performance by being misinterpreted by the controller as reaction forces. The capability of the RTOB-based controller to mitigate these vibrations was explored, revealing that it could significantly enhance system performance.

Overall, this thesis advances the development of motion control systems by presenting a robust solution to the limitations posed by traditional force sensors. The findings demonstrate that RTOB-based controllers can provide variable bandwidth, enhance robustness, and accurately estimate unknown disturbances. Moreover, the recommendations for optimizing controller parameters and the novel parameter estimation technique provide valuable insights for scientists and engineers looking to implement these strategies in their projects.

The study also highlights the importance of vibration suppression, showing that system performance can be effectively improved by using the RTOB-based controller to manage external vibrations. This approach, addressing the shortcomings of force sensors while offering viable solutions for parameter estimation and vibration suppression, can be applied in various settings to enhance the overall effectiveness of motion systems.

Researchers and engineers can further the field of motion control by utilizing the strategies and insights presented in this study, paving the way for more advanced, reliable, and effective motion control applications.

REFERENCES

[1] E. Sariyildiz, "A stability analysis for the reaction torque observer-based sensorless force control systems," in *2023 IEEE International Conference on Mechatronics (ICM)*. IEEE, 2023, pp. 1–5.

[2] Y. Ohba, M. Sazawa, K. Ohishi, T. Asai, K. Majima, Y. Yoshizawa, and K. Kageyama, "Sensorless force control for injection molding machine using reaction torque observer considering torsion phenomenon," *IEEE Transactions on Industrial Electronics*, vol. 56, no. 8, pp. 2955–2960, 2009.

[3] E. Sariyildiz and K. Ohnishi, "A comparison study for force sensor and reaction force observer based robust force control systems," in *2014 IEEE 23rd International Symposium on Industrial Electronics (ISIE)*. IEEE, 2014, pp. 1156–1161.

[4] Z. Qian and Z. Bi, "Recent development of rehabilitation robots," *Advances in Mechanical Engineering*, vol. 7, no. 2, p. 563062, 2015.

[5] G. . L. R. of Stroke Collaborators, "Global, regional, and country-specific lifetime risks of stroke, 1990 and 2016," *New England Journal of Medicine*, vol. 379, no. 25, pp. 2429–2437, 2018.

[6] D. Shi, W. Zhang, W. Zhang, and X. Ding, "A review on lower limb rehabilitation exoskeleton robots," *Chinese Journal of Mechanical Engineering*, vol. 32, no. 1, pp. 1–11, 2019.

[7] S. K. Banala, S. H. Kim, S. K. Agrawal, and J. P. Scholz, "Robot assisted gait training with active leg exoskeleton (alex)," *IEEE transactions on neural systems and rehabilitation engineering*, vol. 17, no. 1, pp. 2–8, 2008.

[8] F. J. Ruiz-Ruiz, J. M. Gandarias, F. Pastor, and J. M. Gomez-De-Gabriel, "Upper-limb kinematic parameter estimation and localization using a compliant robotic manipulator," *IEEE Access*, vol. 9, pp. 48 313–48 324, 2021.

[9] P. Song, Y. Yu, and X. Zhang, "A tutorial survey and comparison of impedance control on robotic manipulation," *Robotica*, vol. 37, no. 5, pp. 801–836, 2019.

[10] M. M. Fateh and R. Babaghasabha, "Impedance control of robots using voltage control strategy," *Nonlinear Dynamics*, vol. 74, pp. 277–286, 2013.

[11] Trisha, G. Gupta, and S. Shiva Kumar, "Review of the parameter estimation and transient analysis of three-phase induction motor," in *Advances in Smart Grid Automation and Industry 4.0: Select Proceedings of ICETSGAI4. 0*. Springer, 2021, pp. 223–232.

[12] S. Katsura, Y. Matsumoto, and K. Ohnishi, "Modeling of force sensing and validation of disturbance observer for force control," *IEEE Transactions on industrial electronics*, vol. 54, no. 1, pp. 530–538, 2007.

[13] B. Ugurlu, M. Nishimura, K. Hyodo, M. Kawanishi, and T. Narikiyo, "Proof of concept for robot-aided upper limb rehabilitation using disturbance observers," *IEEE Transactions on Human-Machine Systems*, vol. 45, no. 1, pp. 110–118, 2014.

[14] R. Ruwanthika and A. H. S. Abeykoon, "3d environmental force: Position impedance variation for different motion parameters," in *2015 Moratuwa Engineering Research Conference (MERCon)*. IEEE, 2015, pp. 112–117.

[15] J. K. Salisbury, "Active stiffness control of a manipulator in cartesian coordinates," in *1980 19th IEEE conference on decision and control including the symposium on adaptive processes*. IEEE, 1980, pp. 95–100.

[16] M. H. Raibert and J. J. Craig, "Hybrid position/force control of manipulators," 1981.

[17] W. Xu, J. Han, and S. Tso, "Experimental study of contact transition control incorporating joint acceleration feedback," *IEEE/ASME transactions on mechatronics*, vol. 5, no. 3, pp. 292–301, 2000.

[18] K. Kim, M. Kang, Y. Choi, H. Jang, J. Han, and C. Han, "Development of the exoskeleton knee rehabilitation robot using the linear actuator," *International Journal of Precision Engineering and Manufacturing*, vol. 13, no. 10, pp. 1889–1895, 2012.

[19] E. Schrijver and J. Van Dijk, "Disturbance observers for rigid mechanical systems: equivalence, stability, and design," *J. Dyn. Sys., Meas., Control*, vol. 124, no. 4, pp. 539–548, 2002.

[20] A. Kato and K. Ohnishi, "Robust force sensorless control in motion control system," in *9th IEEE International Workshop on Advanced Motion Control, 2006.* IEEE, 2006, pp. 165–170.

[21] E. Sariyildiz and K. Ohnishi, "A guide to design disturbance observer," *Journal of Dynamic Systems, Measurement, and Control*, vol. 136, no. 2, p. 021011, 2014.

[22] A. Mohammadi and H. Dallali, "Disturbance observer applications in rehabilitation robotics: an overview," *Powered prostheses*, pp. 113–133, 2020.

[23] P. D. Harischandra and A. H. S. Abeykoon, "Upper-limb tele-rehabilitation system with force sensorless dynamic gravity compensation," *International Journal of Social Robotics*, vol. 11, pp. 621–630, 2019.

[24] X. Su, X. Yan, and C.-L. Tsai, "Linear regression," *Wiley Interdisciplinary Reviews: Computational Statistics*, vol. 4, no. 3, pp. 275–294, 2012.

[25] W. T. G. Wijewardhana, E. H. Senevirathne, and A. H. S. Abeykoon, "Iterative approach for parameter estimation in dc motor based motion systems," in *2020 IEEE 29th International Symposium on Industrial Electronics (ISIE)*. IEEE, 2020, pp. 134–141.

[26] M. Kino, T. Goden, T. Murakami, and K. Ohnishi, "Reaction torque feedback based vibration control in multi-degrees of freedom motion system," in *IECON'98. Proceedings of the 24th Annual Conference of the IEEE Industrial Electronics Society (Cat. No. 98CH36200)*, vol. 3. IEEE, 1998, pp. 1807–1811.

[27] Y. Ali, S. Noor, S. Bashi, and M. Hassan, "Microcontroller performance for dc motor speed control system," in *Proceedings. National Power Engineering Conference, 2003. PECon 2003.* IEEE, 2003, pp. 104–109.

[28] E. Sariyildiz and K. Ohnishi, "Analysis the robustness of control systems based on disturbance observer," *International Journal of Control*, vol. 86, no. 10, pp. 1733–1743, 2013.

[29] ——, "Stability and robustness of disturbance-observer-based motion control systems," *IEEE Transactions on Industrial Electronics*, vol. 62, no. 1, pp. 414–422, 2014.

APPENDIX A

PYTHON BASED SIMULATIONS

A.1 Iterative Approach for Parameter Estimation in DC Motor Based Motion Systems

A.1.1 Parameter declaration and library imports

```
import matplotlib.pyplot as plt
import math
import numpy as np

K_t = 0.135
J = 0.000072
B = 0.02045
T_sf = 0.0182
dt = 200*0.000001
dd_theta_sum = 0.0

K_tn = 0.135
J_n = 0.000072
g_dob = 100
g_rtob = 100
K_p = 5500

dob_after_filter = 0.0
dob_after_filter_sum = 0.0
```

A.1.2 DC Motor model

```
def motor(i_a,T_dis):
  global dd_theta_sum
  T_m = i_a*K_t - T_dis
  dd_theta = T_m/J
  dd_theta_sum = dd_theta_sum + dd_theta*dt
  d_theta = dd_theta_sum
  return d_theta, dd_theta
```

A.1.3 Disturbance Observer Model

```
def dob(i_a,d_theta):
  global dob_after_filter_sum, dob_after_filter
  T_temp = i_a*K_tn + d_theta*J_n*g_dob
  dob_after_filter_sum =dob_after_filter_sum +
     (T_temp-dob_after_filter)*dt
  dob_after_filter = g_dob*dob_after_filter_sum
  T_dis_est = dob_after_filter - d_theta*J_n*g_dob
  return T_dis_est
```

A.1.4 Velocity controller

```
def velocity_controller(v_ref,d_theta):
  v_err = v_ref - d_theta
  i_a = v_err * K_p
  return i_a
```

A.1.5 Main function

```
y = []
ref=[]
velocity_output = []
time = []

i_a=0.0
d_theta = 0.0
X = []

for x in range(1000):
  v_ref = 10 + math.sin(x/2)
  T_dis = B*d_theta + 0.0182

  d_theta, dd_theta = motor(i_a, T_dis)
  i_a = velocity_controller(v_ref,d_theta)

  if (x > 4):
    time.append(x*dt)
    ref.append(v_ref)
    velocity_output.append(d_theta)
```

```
    X.append([1, d_theta , dd_theta])
    T_dis_est = dob(i_a, d_theta)
    y.append(T_dis_est)

plt.plot(time, velocity_output)
plt.plot(time,ref)
plt.show()
```

A.1.6 Newton Raphson Algorithm

```
def nra(theta, X, y):
  m,n = X.shape
  temp1 = np.dot(X,theta)-y
  J_before_sum = (temp1* temp1)/(2*m)
  J = sum(J_before_sum)
  grad = np.dot(np.transpose(X),temp1)/m
  hes = np.dot(np.transpose(X),X)/m
  return J, grad, hes
```

A.1.7 Iterator

```
theta = np.transpose(np.array([0.0, 0.0, 0.0]))
learning_rate = 1
X_array = np.array(X)
y_array = np.array(y)

for iter in range(1, 5):
  J, grad, hes = nra(theta, X_array, y_array)
  theta = theta-learning_rate*np.dot(np.linalg.inv(hes),grad);
```

A.2 Study of stability variations in reaction torque observer-based force controllers

A.2.1 Parameter declaration and library imports

```
import matplotlib.pyplot as plt
import numpy as np

B=0.01
```

```
K_env = 10
J=0.0072
K_p=1000
```

A.3 Define the equation

```
def equation(x, y):
    return ((B+x*J)*(B*y+y*(x+y)*J+K_env)+
    y*J*(B**2+B*y*J-J*K_env)*K_p)/(B+x*J+y*J)
```

A.4 Define the limits of x and y

```
x = np.linspace(100, 800, 1000)
y = np.linspace(100, 900, 1000)
```

A.5 Create a meshgrid from the limits

```
X, Y = np.meshgrid(x, y)
```

A.6 Calculate the Z values for the meshgrid using the equation

```
Z = equation(X, Y)
```

A.7 Create a surface plot

```
fig = plt.figure()
ax = fig.add_subplot(projection='3d')
ax.plot_surface(X, Y, Z, cmap='viridis')
ax.set_xlabel('g_DOB')
ax.set_ylabel('g_RTOB')
ax.set_zlabel('f_1')
plt.show()
```